Quantum photonic integrated circuits

From flying qubits to scalable single-photon technology

Marcin Syperek
Wrocław University of Science and Technology, Poland
3MN centre

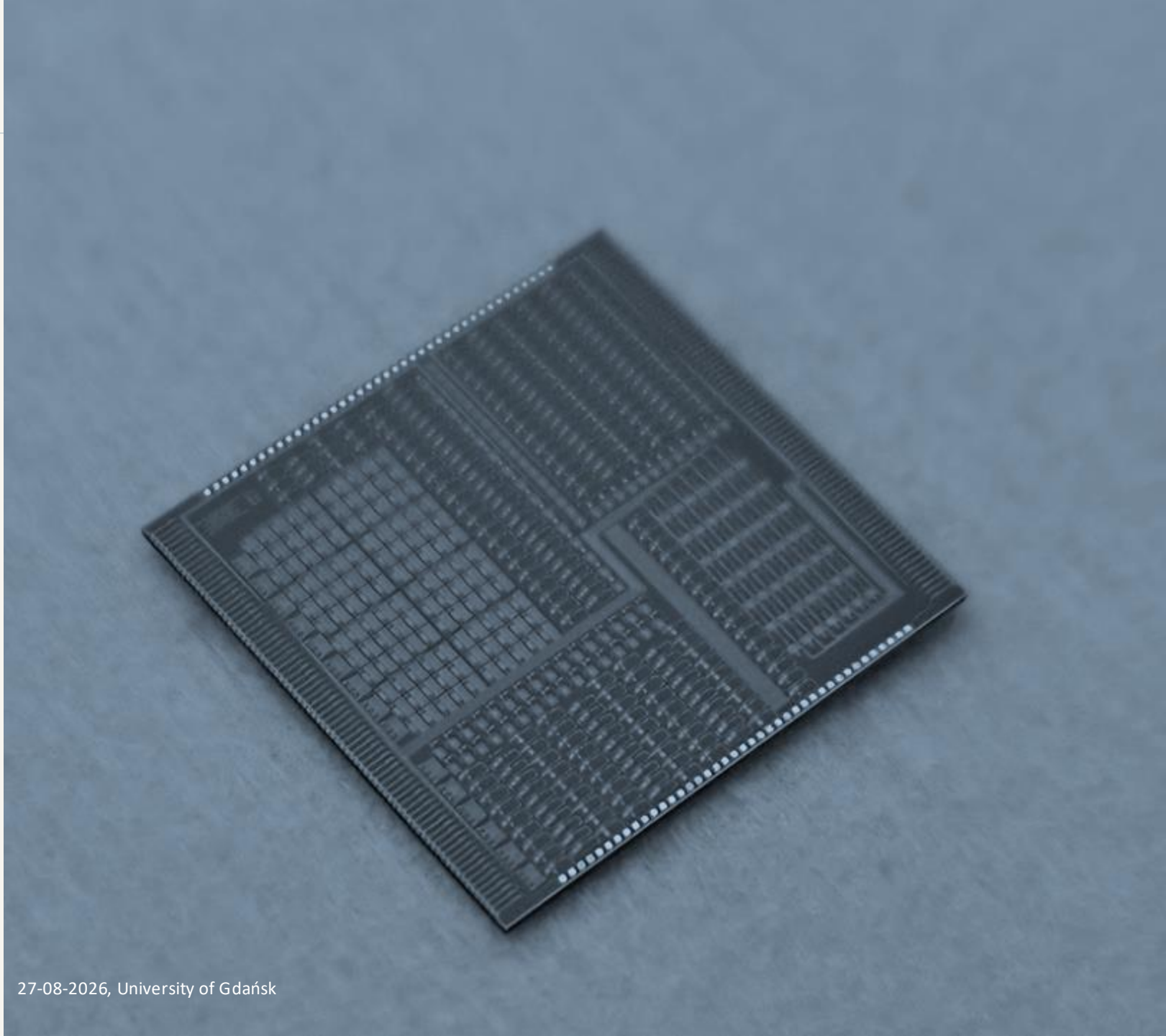

27-08-2026, University of Gdańsk

Quantum photonics must move from the optical table to the chip

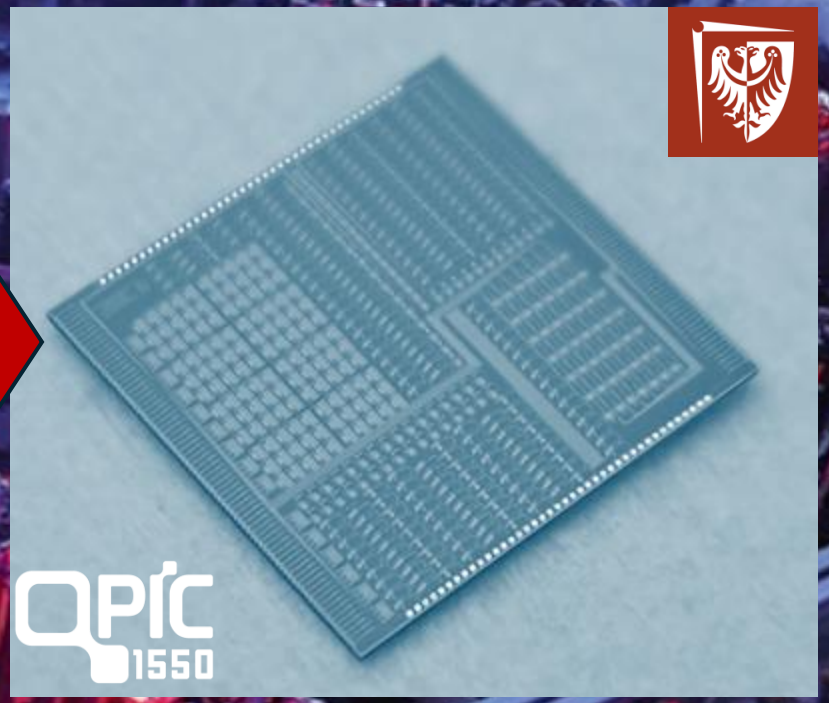

H.-S. Zhong,…,Jlan-Wei Pan “Quantum Computation Advantages using photons” Science 370 (2020)
H.-L Liu,…, Jlan-Wei Pan “Gaussian boson sampling with 1.024 squeezed states in 8.176 modes” Nature 653, 687 (2026)

PART I

Photons as flying qubits

How can a single photon encode a qubit?

Matter qubit vs. Flying qubit (single photon)

MATTER QUBIT

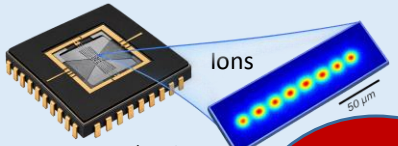

AF: Brown et al. npj Quantum Information 2, 16034 (2016)

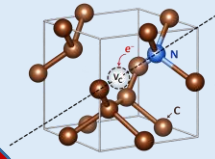

NV center in diamond

Jin et al. npj Computational Materials 8, 238 (2022)

$|0\rangle, |1\rangle$

$|\psi\rangle = \alpha|0\rangle + \beta|1\rangle$

$|\alpha|^2 + |\beta|^2 = 1$

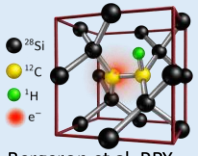

Bergeron et al. PRX Quantum 1, 020301 (2020)

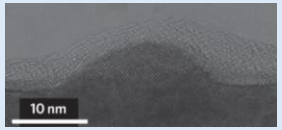

Gao et al. Nature Photonics 9, 363 (2015)

localized

Internal state of a trapped ion:

$|\psi\rangle = \alpha|0\rangle + \beta|1\rangle \rightarrow \ |\psi\rangle_{ion} = \alpha|g\rangle + \beta|e\rangle$

Electron or hole spin in a semiconductor QD:

$|\psi\rangle = \alpha|0\rangle + \beta|1\rangle \rightarrow \ |\psi\rangle_{QD} = \alpha|\uparrow\rangle + \beta|\downarrow\rangle$

NV-centre electron spin in diamond:

$|\psi\rangle = \alpha|0\rangle + \beta|1\rangle \rightarrow \ |\psi\rangle_{NV} = \alpha|m_s = 0\rangle + \beta|m_s = -1\rangle$

Spin defects in Silicon

Matter QUBIT-PHOTON ENTANGLEMENT

hybrid quantum computing

SINGLE PHOTON

linear quantum computing

FLYING QUBIT (single photon)

single-photon temporal mode

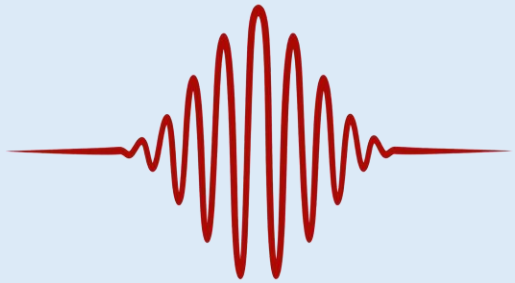

propagates

Information encoded in the two orthogonal modes of a single photon

$|\psi\rangle = \alpha|0\rangle + \beta|1\rangle$

References for hybride quantum computing

Awschalom, D. D. et al., "Quantum technologies with optically interfaced solid-state spins," *Nature Photonics* **12**, 516–527 (2018).
Borregaard, J., Sørensen, A. S., Lodahl, P., "Quantum Networks with Deterministic Spin–Photon Interfaces," *Adv. Quantum Technologies* **2**, 1800091 (2019)
Atatüre, M., Englund, D., Vamivakas, N., Lee, S.-Y., Wrachtrup, J., "Material platforms for spin-based photonic quantum technologies," *Nature Reviews Materials* **3**, 38 (2018).

References for linear quantum computing

Kok, P. et al., "Linear optical quantum computing with photonic qubits," *Reviews of Modern Physics* **79**, 135–174 (2007).
Flamini, F., Spagnolo, N. & Sciarrino, F., "Photonic quantum information processing: a review," *Reports on Progress in Physics* **82**, 016001 (2019).

Different ways to encode a qubit in a single photon

General two-mode qubit state

$$|\psi\rangle = \alpha|0\rangle + \beta e^{i\phi}|1\rangle$$

$$|\alpha|^2 + |\beta|^2 = 1$$

$$|\psi\rangle = cos\frac{\theta}{2}|0\rangle + e^{i\phi}sin\frac{\theta}{2}|1\rangle$$

Two-mode qubit state preparation on the Bloch sphere

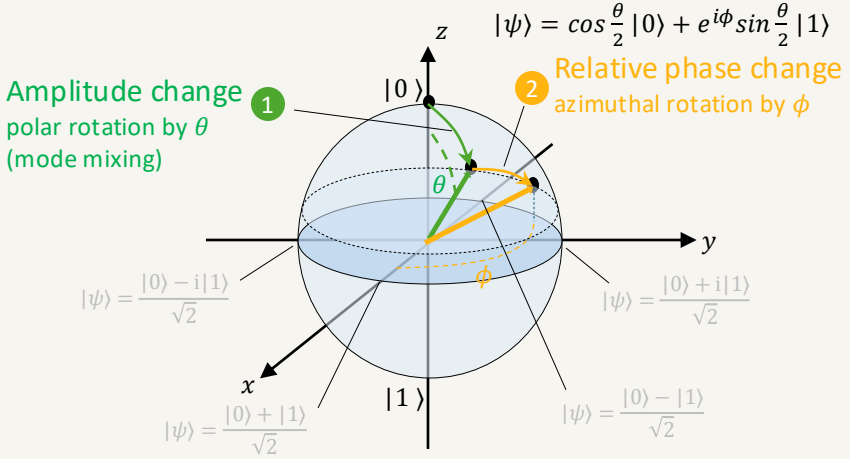

All two-mode encodings share the same qubit Hilbert space

Polarization encoding

$$|\psi\rangle_{pol} = \alpha|H\rangle + \beta e^{i\phi}|V\rangle$$

A single photon encodes a qubit in two orthogonal polarization modes.

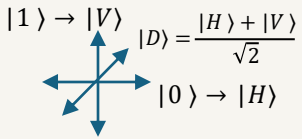

Path (dual-rail) encoding

$$|\psi\rangle_{path} = \alpha|u\rangle + \beta e^{i\phi}|l\rangle$$

A single photon is encoded in a superposition of two spatial modes

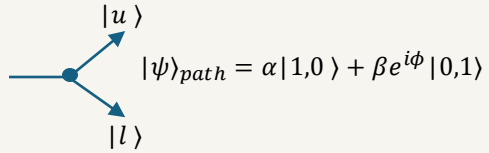

Time-bin encoding

$$|\psi\rangle_{time} = \alpha|early\rangle + \beta e^{i\phi}|late\rangle$$

A single photon is prepared in a coherent superposition of two distinguishable temporal modes

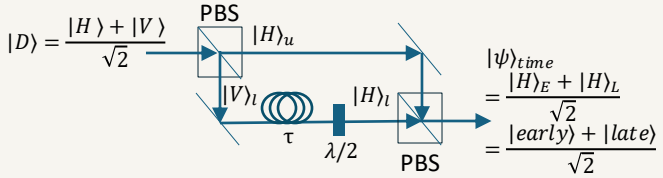

Frequency-bin encoding

$$|\psi\rangle_{freq} = \alpha|\omega_0\rangle + \beta e^{i\phi}|\omega_1\rangle$$

$$\omega_1 = \omega_0 + \Delta\omega$$

A single photon is prepared in a coherent superposition of two discrete frequency modes

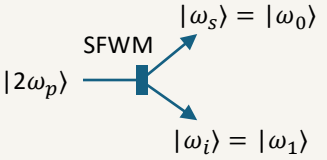

- P. Kok, et al., *Linear optical quantum computing with photonic qubits*, *Reviews of Modern Physics* 79, 135 (2007)
- J. L. O'Brien *Optical Quantum Computing* *Science* 318, 1567–1570 (2007)
- J. L. O'Brien, A. Furusawa, J. Vučković *Photonic quantum technologies* *Nature Photonics* **3**, 687–695 (2009)

Processor operations: single-qubit gates (examples)

Single-qubit gates correspond to rotations of the photonic qubit state on the Bloch sphere

Single-qubit gate	Function	Operation	Example (polarization encoding)
X	Flip qubit/exchange modes	$\alpha\|0\rangle+\beta e^{i\phi}\|1\rangle \xrightarrow{X} \beta e^{i\phi}\|0\rangle+\alpha\|1\rangle, \theta'\to\pi-\theta, \phi'=-\phi$	$\|H\rangle\to\|V\rangle, \|D\rangle\to\|D\rangle, \|A\rangle\to-\|A\rangle$ $\lambda/2$, polarization rotator
Z	Apply a π phase shift between logical modes	$\alpha\|0\rangle+\beta e^{i\phi}\|1\rangle \xrightarrow{Z} \alpha\|0\rangle-\beta e^{i\phi'}\|1\rangle, \theta'\to\theta, \phi'=\phi+\pi$	$\|H\rangle\to\|H\rangle, \|V\rangle\to-\|V\rangle, \|D\rangle\to\|A\rangle$ Phase shifter
$R(\varphi)$	Relative phase rotation around z-axis	$\alpha\|0\rangle+\beta e^{i\phi}\|1\rangle \xrightarrow{R(\varphi)} \alpha\|0\rangle+\beta e^{i(\phi+\varphi)}\|1\rangle$	$\|D\rangle\to\|\sigma\rangle, \left(\frac{\|H\rangle+\|V\rangle}{\sqrt{2}}\to\frac{\|H\rangle+\mathrm{i}\|V\rangle}{\sqrt{2}}\right)$
$(H)Hadamard$	Mixes modes (implemented as a beam splitter)	$\mathrm{H}\|0\rangle=\frac{\|0\rangle+\|1\rangle}{\sqrt{2}} \quad \mathrm{H}\|1\rangle=\frac{\|0\rangle-\|1\rangle}{\sqrt{2}}$ $\alpha\|0\rangle+\beta e^{i\phi}\|1\rangle \xrightarrow{H} \frac{\alpha+\beta e^{i\phi}}{\sqrt{2}}\|0\rangle+\frac{\alpha-\beta e^{i\phi}}{\sqrt{2}}\|1\rangle$	$\|H\rangle\to\|D\rangle, \|V\rangle\to\|A\rangle$

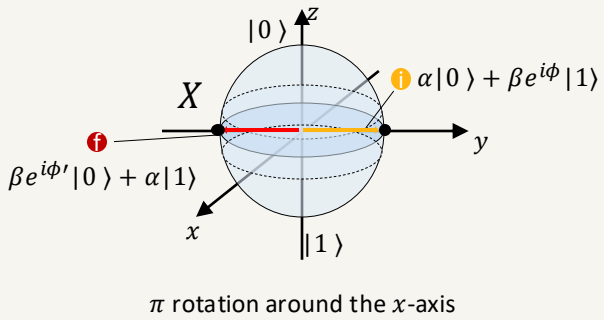

π rotation around the x-axis

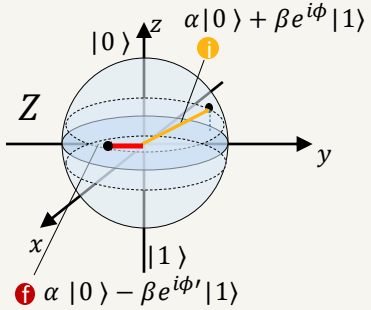

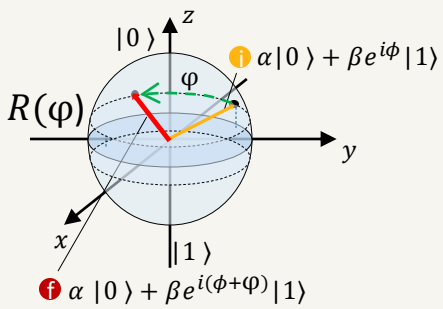

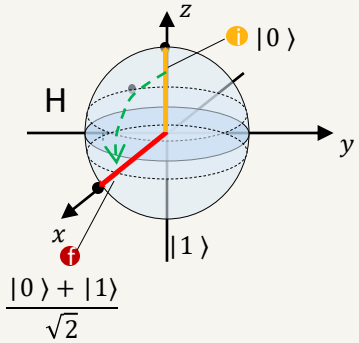

Processor operations: two-qubit gates and entangling operations

Two-qubit gates create correlations and entanglement between photonic qubits.

two-qubit gate	Function	Operation
CZ	Change the phase of d by π	$a\|00\rangle + b\|01\rangle + c\|10\rangle + d\|11\rangle \xrightarrow{CZ} a\|00\rangle + b\|01\rangle + c\|10\rangle - d\|11\rangle, d \to de^{i\pi} = -d$
$CP(\varphi)$ controlled phase	$\|11\rangle$ gets the phase φ relative to other components	$a\|00\rangle + b\|01\rangle + c\|10\rangle + d\|11\rangle \xrightarrow{CP} a\|00\rangle + b\|01\rangle + c\|10\rangle + de^{i\phi}\|11\rangle, d \to de^{i\phi}$
$CNOT$	Permutes the amplitude c and d	$a\|00\rangle + b\|01\rangle + c\|10\rangle + d\|11\rangle \xrightarrow{CNOT} a\|00\rangle + b\|01\rangle + d\|10\rangle + c\|11\rangle, d \to c, c \to d$
$SWAP$	Exchange qubit states (b and c)	$a\|00\rangle + b\|01\rangle + c\|10\rangle + d\|11\rangle \xrightarrow{SWAP} a\|00\rangle + c\|01\rangle + b\|10\rangle + c\|11\rangle, c \leftrightarrow b$
$Bell\ measurment$	Project onto entangled basis	
$Fusion\ gate$	Measurement-induced entangling operation used for cluster-state generation	

Unlike single-qubit operations, two-qubit gates require interaction between photons or measurement-induced nonlinearities.

PART II

Linear optical quantum computing architecture

How can we compute with photons that do not directly interact?

Functional architecture of a photonic linear quantum computer

Classical Control and Feed-forward

Real-time synchronization and adaptive control
(phase stabilization, thermo-optic and EO tuning, detector timing, feed-forward corrections)

GENERATE

One photon per trigger
- On-demand generation
- High indistinguishability
- High extraction efficiency
- controlled spectrum
- Controller temporal wavepacket
- Defined spatial mode

$$|\psi\rangle = |0\rangle$$

INIT/ENCODE

Encode a logical qubit into a photon degree of freedom

$|0\rangle, |1\rangle \rightarrow H/V, u/l, early/late, \omega_0/\omega_1$

$$|\psi\rangle_{in} = cos\frac{\theta}{2}|0\rangle + e^{i\phi}sin\frac{\theta}{2}|1\rangle$$

- Polarization rotator (θ)
- Tunable coupler (θ)
- Phase shifters (ϕ)

PROCESS

- single-qubit unitary operations
- multi-photon interference
- entangling gates/measurement-induced nonlinearities

$$|\psi\rangle_{out} = U|\psi\rangle_{in}$$

- Beam splitters
- Phase shifters
- Interferometers

MEASURE

Project the quantum state onto the measurement basis and record detection events

- Photon number resolution
- Time resolution

$$|\psi\rangle_{out} \rightarrow classical\ outcome$$

- Single photon detectors
- Photon number detector
- Time-tagger

Physical layer

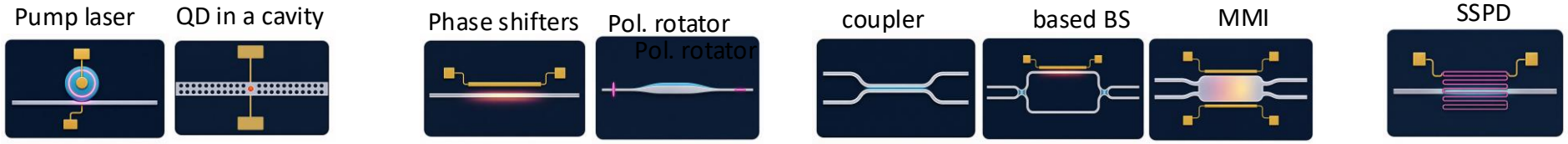

J. Wang et al., *Integrated photonic quantum technologies* *Nature Photonics* 14, 273 (2020)
E. Knill, R. Laflamme, G. J. Milburn *Scheme for efficient quantum computation with linear optics* *Nature* **409**, 46 (2001)
P. Kok, et al., *Linear optical quantum computing with photonic qubits*, *Reviews of Modern Physics* 79, 135 (2007)

Scalable photonic computing requires the right number of photons per clock cycle

Probability of generating n photons per trigger pulse

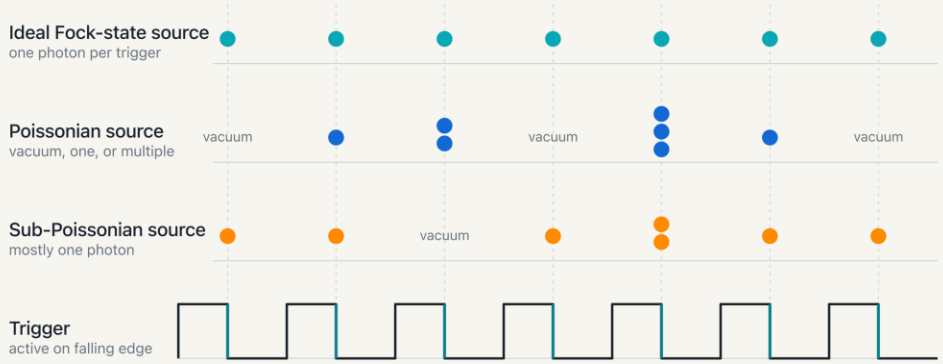

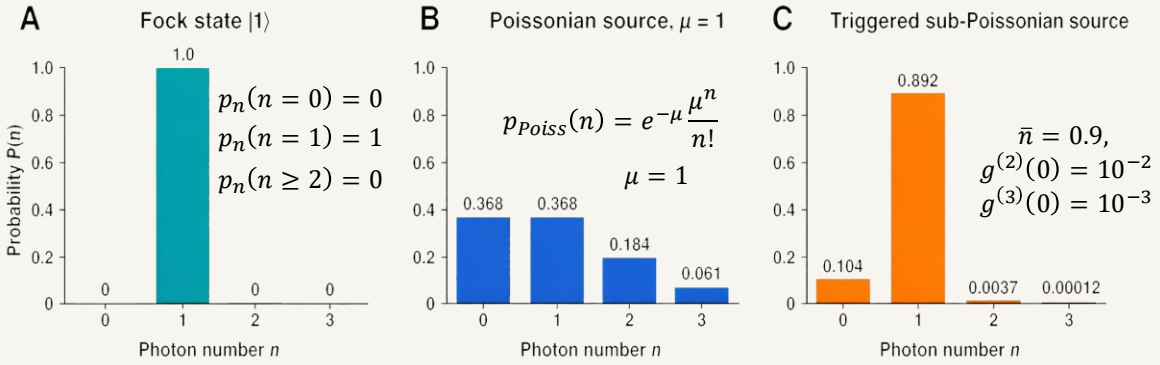

An ideal source

A strongly dumped laser source

Triggered sub-Poissonian source

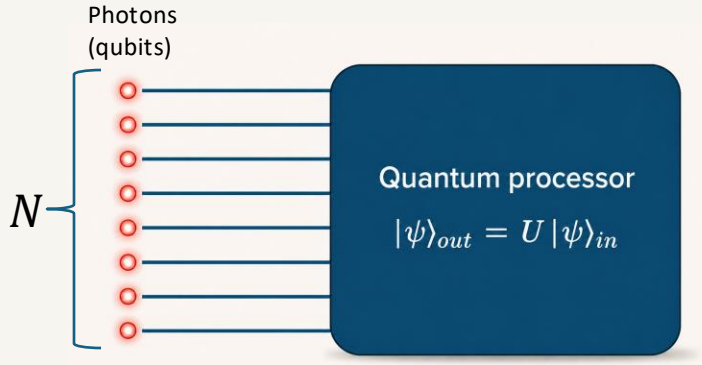

Prob. of having N photons at the input

Prob. of generating n photons by the source

Chip transmission

$$P_{All}(N)=(p_n\eta)^N$$

Mean time of having N photons at the processor

Photon generation rate

$$\langle t\rangle=\frac{1}{RP_{All}(N)}$$

SOURCE	$p_{n=1}$	N	$P_{All}(N)$ **	MEAN TIME*
Fock	1	4	1	$1\,ns$
Fock	1	8	1	$1\,ns$
Poisson, $\mu=1$	0.368	4	0.018	$54.6\,ns$
Poisson, $\mu=1$	0.368	8	0.0003355	$2.98\,\mu s$
sub-Poissonian	0.892	4	0.6338	$1.58\,ns$
sub-Poissonian	0.892	8	0.4017	$2.49\,ns$

*$R=1GHz$

**$\eta=1$

M. Pant et al. *Percolation thresholds for fault-tolerant photonic quantum computing* Nature Photonics **14**, 256 (2020)
N. Tomm et al. *A bright and fast source of coherent single photons* Nature Nanotechnology **16**, 399 (2021)
X. Ding, et al. *High-efficiency single-photon source above the loss-tolerant threshold for efficient linear optical quantum computing* Nature Photonics **19**, 387, (2025)

Indistinguishable photons are required for high-fidelity quantum operations

A photon, time-domain representation

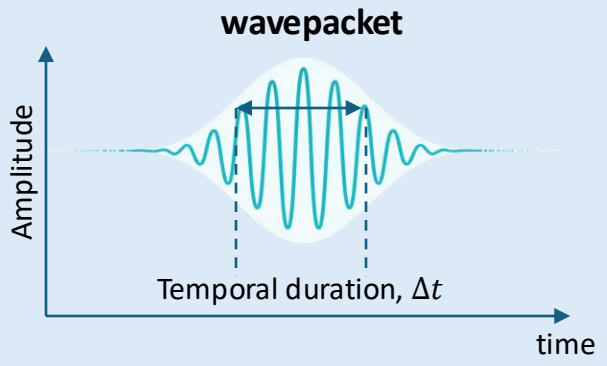

Fourier transform

A photon, frequency-domain representation

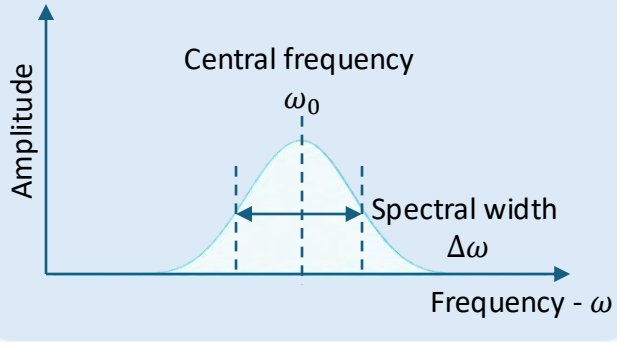

For single-photon operations, indistinguishability between photons is not required

(but it requires coherence, spectral stability, and mode purity)

What does indistinguishability mean?

$$|\psi\rangle_A = |\psi\rangle_{A,logic} \otimes |\varphi\rangle_{A,aux}$$

$$|\psi\rangle_B = |\psi\rangle_{B,logic} \otimes |\varphi\rangle_{B,aux}$$

$|\psi\rangle_{A,logic}$ and $|\psi\rangle_{B,logic}$ **can be different BUT** $|\varphi\rangle_{A,aux} \approx |\varphi\rangle_{B,aux}$

Indistinguishability:

- central frequency and spectral bandwidth: $\omega_{A,0} \approx \omega_{B,0}$, $\Delta\omega_A \approx \Delta\omega_B$
- arrival time and temporal envelope: $t_{A,0} \approx t_{B,0}$, $\Delta t_{A,0} \approx \Delta t_{B,0}$
- spatial waveguide mode
- polarization state (unless polarization encodes the qubit)
- coherence and phase stability

Quantifying indistinguishability:

$$M = \left|\langle |\varphi\rangle_{A,aux} | |\varphi\rangle_{B,aux} \rangle\right|^2$$

mode overlap/indistinguishability parameter

$M = 1$: perfect indistinguishability
$M = 0$: perfect distinguishability
$0 < M < 1$: partial indistinguishability

How to measure indistinguishability -> Hong-Ou-Mandel interference

C. K. Hong, Z. Y. Ou, L. Mandel, *Measurement of Subpicosecond Time Intervals between Two Photons by Interference* Phys. Rev. Lett. 59, 2044 (1987)

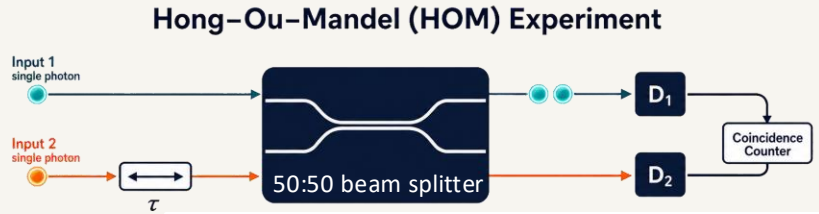

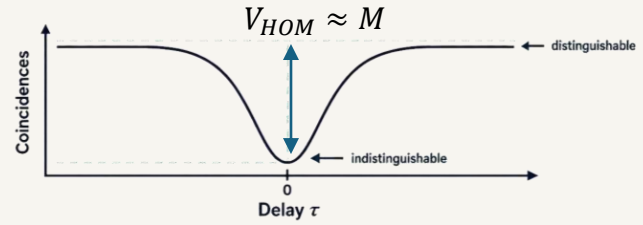

Indistinguishable photons interfere and exit the same output port (bosonic coalescence).

Two-photon interference: Hong–Ou–Mandel effect

C. K. Hong, Z. Y. Ou, L. Mandel, *Measurement of Subpicosecond Time Intervals between Two Photons by Interference* Phys. Rev. Lett. 59, 2044 (1987)
H. Fearn and R. Loudon, *Theory of two-photon interference* JOSA B 6, 917 (1989)
L. Mandel, *Coherence and indistinguishability* Opt. Lett. 16, 1882 (1991)
T. Legero et al., *Time-resolved two-photon quantum interference* Appl. Phys. B 77, 797 (2003)

Unlike classical interferometers, HOM interference is not sensitive to the optical phase between paths, it arises from interference between two-photon probability amplitudes.

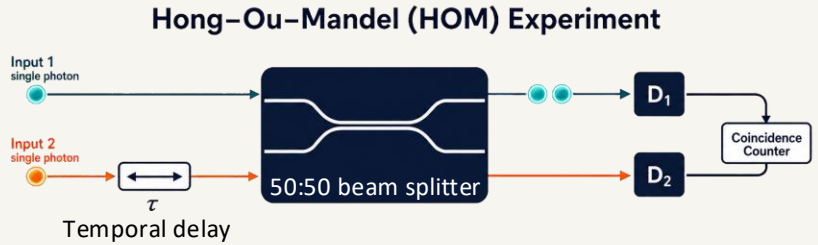

Possible outputs:

$|n_1, n_2\rangle$- photon number states at the two outpu ports
$|2,0\rangle$- two photons in the upper line
$|1,1\rangle$- one photon in the upper line, one in the lower
$|0,2\rangle$- two photons in the lower line

Losless 50/50 beam splitter:

Single-photon quantum probability amplitude for transmission: $A_T = \frac{1}{\sqrt{2}}$

Single-photon quantum probability amplitude for reflecton: $A_R = \frac{-i}{\sqrt{2}}$

(The amplitudes have a relative phase $A_R = -\mathrm{i}A_T$)

Distinguishable photons

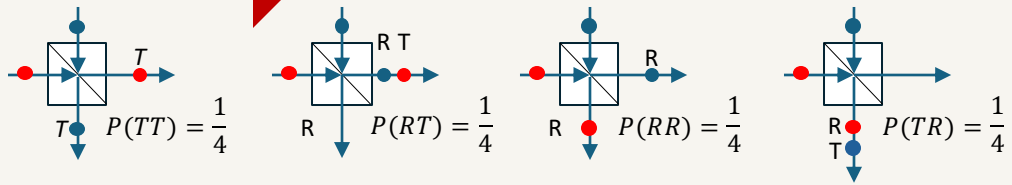

$|2,0\rangle \rightarrow P_{RT} = |A_R \times A_T|^2 = \left|\frac{-i}{2}\right|^2 = \frac{1}{4}$

$|1,1\rangle \rightarrow P_{TT} = |A_T \times A_T|^2 = \frac{1}{4}, P_{RR} = |A_R \times A_R|^2 = \frac{1}{4}$

$|0,2\rangle \rightarrow P_{TR} = |A_T \times A_R|^2 = \frac{1}{4}$

$P_{|1,1\rangle} = P_{TT} + P_{RR} = 1/2$

When photons are distinguishable, one can add probabilities

Indistinguishable photons

When photons are distinguishable, the alternatives do not interfere and probabilities add

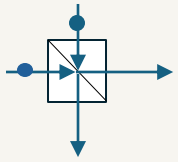

Two photons transmitted: $A_{TT} = A_T \times A_T = \left(\frac{1}{\sqrt{2}}\right)^2 = +\frac{1}{2}$

Two photons reflected: $A_{RR} = A_R \times A_R = \left(\frac{-i}{\sqrt{2}}\right)^2 = -\frac{1}{2}$

One photon reflected/transmitted one transmitted/reflected:

$A_{RT} = A_R \times A_T = \frac{-i}{\sqrt{2}} \times \frac{1}{\sqrt{2}} = -\frac{i}{2}$ $A_{TR} = A_T \times A_R = \frac{1}{\sqrt{2}} \times \frac{-i}{\sqrt{2}} = -\frac{i}{2}$

A_{TT} and A_{RR} produce the same final state: $|1,1\rangle$

$A_{|1,1\rangle} = A_{TT} + A_{RR} = \frac{1}{2} - \frac{1}{2} = 0$

$|2,0\rangle \rightarrow P_{|2,0\rangle} = \left|\sqrt{2}A_T A_R\right|^2 = \frac{1}{2}$

$|1,1\rangle \rightarrow P_{|1,1\rangle} = 0$

$|0,2\rangle \rightarrow P_{|0,2\rangle} = \left|\sqrt{2}A_T A_R\right|^2 = \frac{1}{2}$

bosonic normalization factor - two identical photons occupy the same state

When photons are indistinguishable, first add amplitudes, then calculate probability. Photons exit through the same output port (photon bunching).

Two-photon interference: Hong–Ou–Mandel effect

The HOM experiment does not directly detect photon bunching - it measures the suppression of coincidence events: $|1,1\rangle \rightarrow P_{coinc} \rightarrow 0$

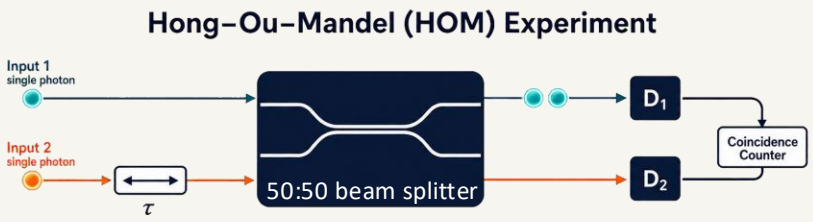

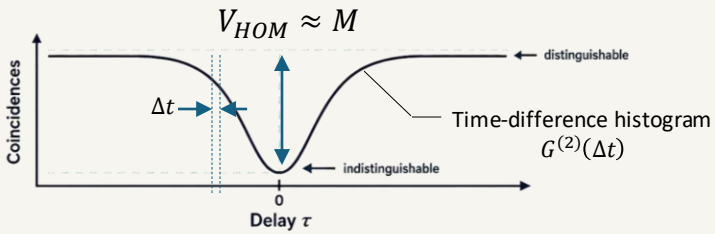

Photon bunching: suppression of coincidence detection

The number of 2-photon trials / detector 1 efficiency

$$C = Ntri_{als} P_{coinc} \eta_1 \eta_2 = N \frac{1}{2}\left(1 - M(\tau)\right)\eta_1 \eta_2$$

Coincidence probability / detector 2 efficiency

For a 50:50 beam splitter: $P_{coinc}^{50:50} = \frac{1}{2}(1 - M)$ (Photon wavepacket overlap)

Photon wavepacket overlapp	P_{coinc}	Coincidences – C (per 10^3 trials)
$M = 0$ (full distinguishability)	0.5	500
$M = 0.5$ (partial distinguishability)	0.25	250
$M = 1$ (full indistinguishability)	0	0

$$V_{HOM} = \frac{C_{dist} - C_{indist}}{C_{dist}}$$

$C_{dist} = 10^4, C_{indist} = 10^3,$
$V_{HOM} = 0.9 \rightarrow V_{HOM} = 90\% \rightarrow M = 90\%$

In a real experiment $V_{HOM} < M$ due to multiphoton emission, background, detector timing jitter and imperfect mode matching

C. K. Hong, Z. Y. Ou, L. Mandel, *Measurement of Subpicosecond Time Intervals between Two Photons by Interference* Phys. Rev. Lett. 59, 2044 (1987)
H. Fearn and R. Loudon, *Theory of two-photon interference* JOSA B 6, 917 (1989)
L. Mandel, *Coherence and indistinguishability* Opt. Lett. 16, 1882 (1991)
T. Legero et al., *Time-resolved two-photon quantum interference* Appl. Phys. B 77, 797 (2003)

From building blocks to a photonic quantum processor

Ancila is a cloud-accessible platform using an on-demand quantum-dot single-photon source, programmable demultiplexing, a 12-mode universal interferometer, and photon detection/post-processing. The platform operates up to 6 single photons, path-encoded into 12-mode universal interferometer.

Number of qubits	Gate operation fidelity
1	99.6(0.1)%
2	93.8(0.6)%
3	86.0(1.2)%

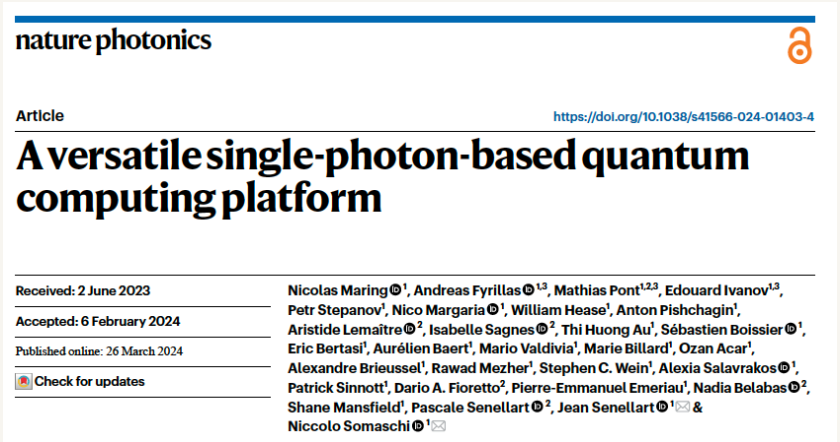

nature photonics

Article https://doi.org/10.1038/s41566-024-01403-4

A versatile single-photon-based quantum computing platform

Received: 2 June 2023

Accepted: 6 February 2024

Published online: 26 March 2024

Check for updates

Nicolas Maring[1], Andreas Fyrillas[1,3], Mathias Pont[1,2,3], Edouard Ivanov[1,3], Petr Stepanov[1], Nico Margaria[1], William Hease[1], Anton Pishchagin[1], Aristide Lemaître[2], Isabelle Sagnes[2], Thi Huong Au[1], Sébastien Boissier[1], Eric Bertasi[1], Aurélien Baert[1], Mario Valdivia[1], Marie Billard[1], Ozan Acar[1], Alexandre Brieussel[1], Rawad Mezher[1], Stephen C. Wein[1], Alexia Salavrakos[1], Patrick Sinnott[1], Dario A. Fioretto[2], Pierre-Emmanuel Emeriau[1], Nadia Belabas[2], Shane Mansfield[1], Pascale Senellart[2], Jean Senellart[1] ✉ & Niccolo Somaschi[1] ✉

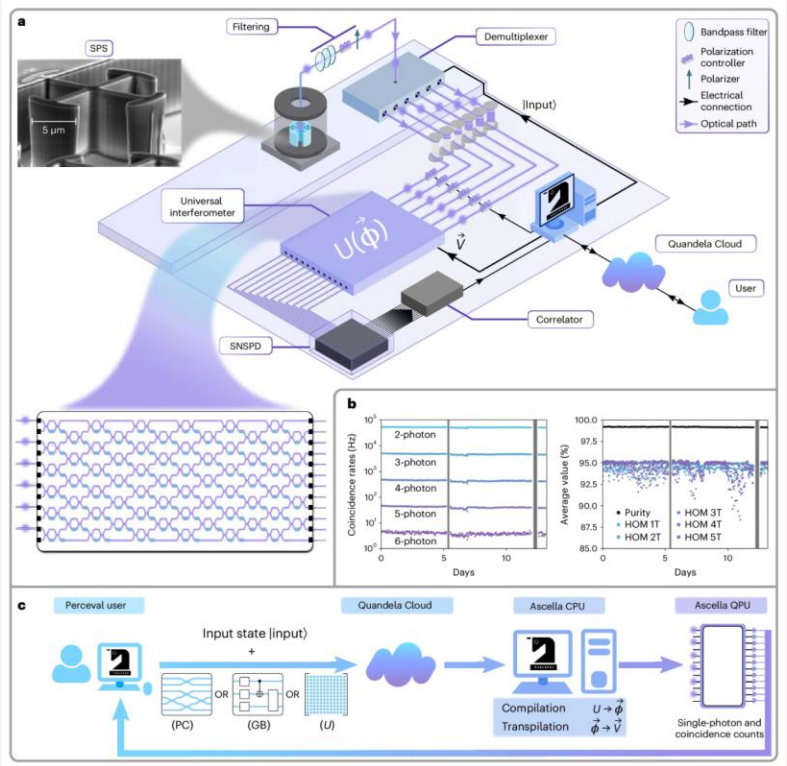

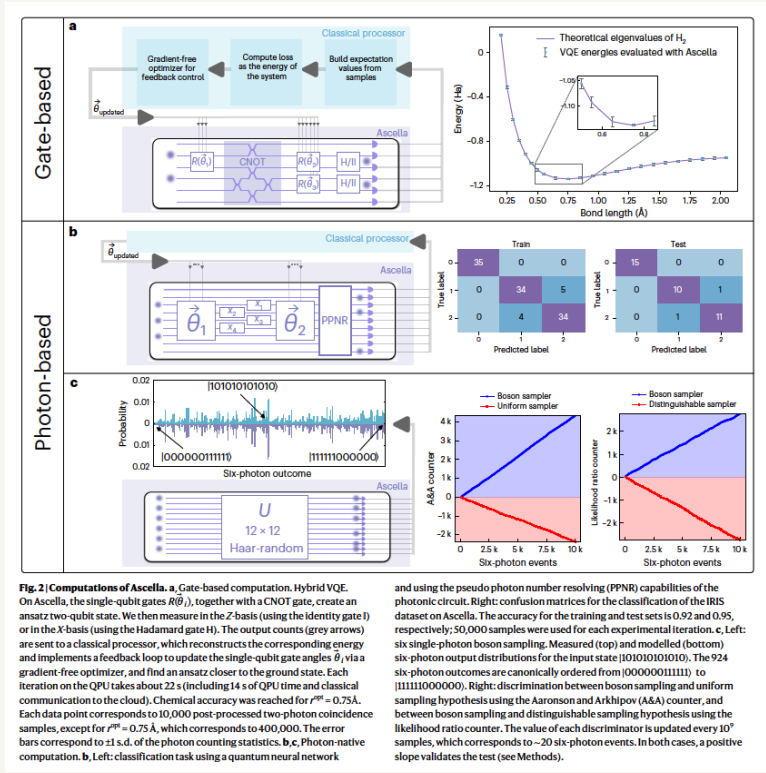

Fig. 2 | Computations of Ascella. a, Gate-based computation. Hybrid VQE. On Ascella, the single-qubit gates $R(\vec{\theta}_i)$, together with a CNOT gate, create an ansatz two-qubit state. We then measure in the Z-basis (using the identity gate I) or in the X-basis (using the Hadamard gate H). The output counts (grey arrows) are sent to a classical processor, which reconstructs the corresponding energy and implements a feedback loop to update the single-qubit gate angles $\vec{\theta}_i$ via a gradient-free optimizer, and find an ansatz closer to the ground state. Each iteration on the QPU takes about 22 s (including 14 s of QPU time and classical communication to the cloud). Chemical accuracy was reached for r^{opt} = 0.75 Å. Each data point corresponds to 10,000 post-processed two-photon coincidence samples, except for r^{opt} = 0.75 Å, which corresponds to 400,000. The error bars correspond to ±1 s.d. of the photon counting statistics. **b**,**c**, Photon-native computation. **b**, Left: classification task using a quantum neural network and using the pseudo photon number resolving (PPNR) capabilities of the photonic circuit. Right: confusion matrices for the classification of the IRIS dataset on Ascella. The accuracy for the training and test sets is 0.92 and 0.95, respectively; 50,000 samples were used for each experimental iteration. **c**, Left: six single-photon boson sampling. Measured (top) and modelled (bottom) six-photon output distributions for the input state |101010101010⟩. The 924 six-photon outcomes are canonically ordered from |000000111111⟩ to |111111000000⟩. Right: discrimination between boson sampling and uniform sampling hypothesis using the Aaronson and Arkhipov (A&A) counter, and between boson sampling and distinguishable sampling hypothesis using the likelihood ratio counter. The value of each discriminator is updated every 10^3 samples, which corresponds to ~20 six-photon events. In both cases, a positive slope validates the test (see Methods).

A photonic processor is an integrated system: source quality+mode control+interference+detection_classical control

PART III

Passive and active photonic circuits

What functions can already be fabricated reliably on a chip?

Integration turns a chain of optical functions into one stable platform

Chip function	Passive component	Active version	Control/tuning mechanism	Role
Qubit transport	Single-/multi-mode waveguide	Thermo-optically/electro-optically tuned waveguide	Geometry/refractive index tuning	Qubit routing and phase accumulation/control
Photons splitting/interfering	Directional coupler, MMI	Tunable coupler, MZI with phase shifter	Coupling strength/relative phase	Photons splitting, interfering, HOM, quantum gates, programmable splitting ratio
Phase control	Fixed phase delay/path-length imbalance	Thermo-optic or electro-optic phase shifter	Optical path length/refractive-index tuning	Controls relative optical phase, programmable quantum gate operation
Spectral processing	Ring resonator, Bragg grating, AWG	Tunable ring resonators and filters, EO frequency shifter	Resonance/spectra-filter tuning	Spectral filtering, wavelength routing and demultiplexing
I/O coupling	Edge grating, or waveguide coupler		Fixed geometry/mode matching	Coupling between fiber/free space, on-chip source and waveguides
Photon source		QD, colot center/defect, SPDC or SFWM source	Optical or electrical excitation	Deliver single photons
Modulation		EO/amplitudę/frequency modulator	Electro-optic / carrier-induced index or absorption change	Dynamically controls phase, amplitudę, frequency or temporal mode
Detection		Superconducting nanowire single photon detector (SNSPD), single photon avalanche diode (SPAD), photodiode	Electric bias and redout	Performs quantum measurement and photon-numer/click detection

STABILITY

fixed optical paths

COMPACTNESS

many functions per chip

REPRODUCIBILITY

lithographic definition

LOWER LOSS

fewer interfaces

Material platform comparison

Platform	n@1550 nm	Useful spectral range	Typ. propagation loss	Optical mode confinement	fast EO/Thermo-optic	Ket advantage for QPIC
Si/SiO_2 (SOI)	$\sim 3.48/1.17$	$\sim 1.1 - 4\ \mu m$	$(0.1 - 3)\ dB/cm$ $(2.3 - 50)\ \%/cm$	$Si/SiO_2\ \Delta n \sim 2.04\ (59\%)$	Yes (conditional)/high	Very compact, CMOS scalable
Si_3N_4	~ 1.98	$\sim 0.4 - 4\ \mu m$	$< 0.1\ dB/cm$ $< 2.3\ \%/cm$	$Si_3N_4/SiO_2\ \Delta n \sim 0.54\ (27\%)$	No/moderate	Ultra-low-loss passive circuits
$LiNbO_3$	$\sim 2.14 - 2.21$	$\sim 0.4 - 5\ \mu m$	$(< 0.02 - 0.5)\ dB/cm$ $(< 0.5 - 11)\ \%/cm$	$LiNbO_3/SiO_2\ \Delta n \sim 0.7\ (33\%)$	Yes, ultrafast/low-moderate	Low-loss, ultrafast EO control
InP	~ 3.17	$\sim 0.9 - 16\ \mu m$	$(0.5 - 3)\ dB/cm$ $(11 - 50)\ \%/cm$	$InP/SiO_2\ \Delta n \sim 1.73\ (55\%)$ $InP/InGaAsP\ \Delta n \sim 0.18\ (5\%)$	yes/moderate	Efficient light sources
AlN	$\sim 2.04 - 2.08$	$\sim 0.2 - 13\ \mu m$	$(\sim 0.14 - 0.6)\ dB/cm$ $(\sim 0.3 - 13)\ \%/cm$	$AlN/SiO_2\ \Delta n \sim 0.6$	Yes, v. fast/	Piezoelectric -> phonons
GaAs	~ 3.38	$\sim 0.9 - 17\ \mu m$	$< 1\ dB/cm$ $< 21\ \%/cm$	$GaAs/AlGaAs\ \Delta n \sim 1.24$	Yes, fast/	Very versatile platform
Ta_2O_5	~ 2.05	$\sim 0.28 - 9\ \mu m$	$(0.07 - 0.7)\ dB/cm$ $(1.6 - 15)\ \%/cm$	$Ta_2O_5/SiO_2 \Delta n \sim 0.61$	Yes/	Very versatile platform,ultra low loss

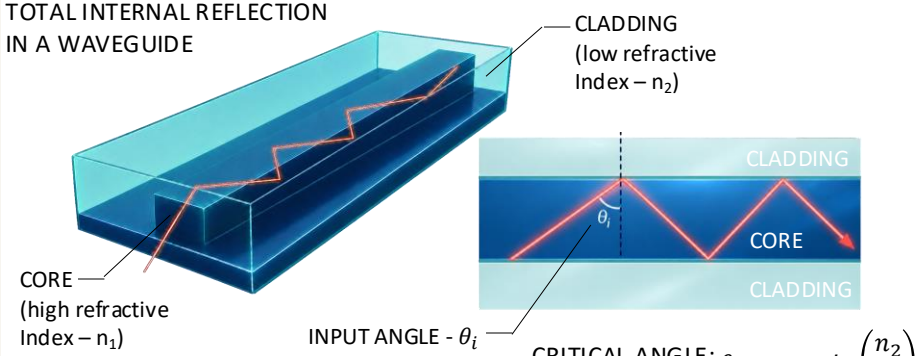

Si/SiO_2

$\theta_c = 24.4° \rightarrow 24.4° < \theta_i < 90°$

SiN/SiO_2

$\theta_c = 47° \rightarrow 47° < \theta_i < 90°$

$InP/InGaAsP$

$\theta_c = 70° \rightarrow 70° < \theta_i < 90°$

CONDITION FOR THE MODE CONFINEMENT

$$n_{CORE} > n_{CLADDING}$$

$$\Delta n = n_{CORE} - n_{CLADDING}$$

$\Delta n \uparrow \xrightarrow{\text{yields}}$ stronger mode confinement

From material to a single mode operation

WAVEGUIDE, FUNDAMENTAL PARAMETERS

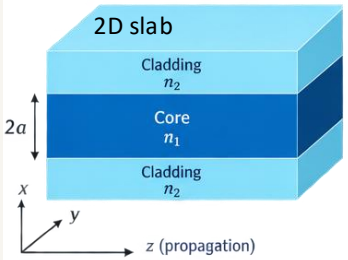

Normalized frequency

The V can be seen as the optical size of the waveguide. It combines geometry, wavelength, and index contrast

$$V = \frac{2\pi a}{\lambda}\sqrt{n_{core}^2 - n_{cladding}^2}$$

a: half core thickness; λ: free-space wavelength

$V < \frac{\pi}{2}$ - single-mode waveguide $V = \frac{\pi}{2}$ -TE_0 cut-off $V > \frac{\pi}{2}$ - multi-mode WG

$$V = const \rightarrow \Delta n \nearrow \; and \; a \searrow$$

Katsunari Okamoto, "Fundamentals of Optical Waveguides" 3rd edition, Academic Press, 2022
A. W. Snyder and J. D. Love, "Optical Waveguide Theory", Chapman & Hall, 1983

MODE STRUCTURE IN A WAVEGUIDE

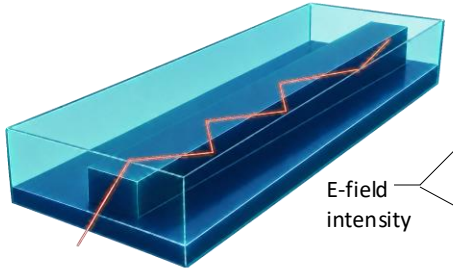

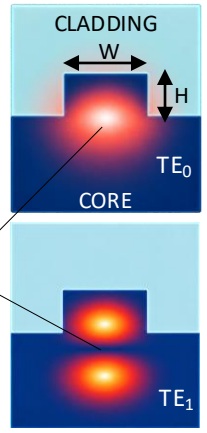

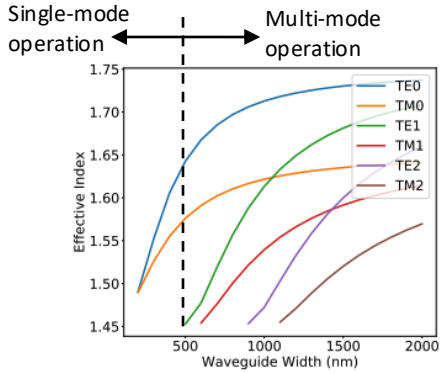

Martin Sinclair PhD Thesis, Univ. Glasgow

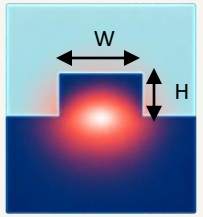

Typical dimensions of a single-mode waveguide @1550 nm

Material	W×H	Δn
Si/SiO_2	~450 nm×220 nm	59%
InP/SiO_2	~500 nm×250 nm	55%
SiN/SiO_2	~850 nm×400 nm	27%
InP/InGaAsP	~3-4μm ×500 nm	5%

$$V = const \rightarrow \Delta n \nearrow \; and \; a \searrow$$

Need a **lithography process** with sufficient:

- critical-dimension resolution
- dimensional control
- overlay accuracy
- edge roughness control

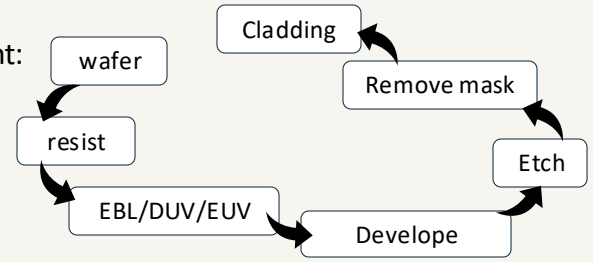

From material to a single mode operation

WAVEGUIDE, FUNDAMENTAL PARAMETERS

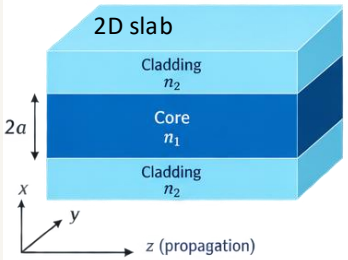

Normalized frequency

The V can be seen as the optical size of the waveguide. It combines geometry, wavelength, and index contrast

$$V = \frac{2\pi a}{\lambda}\sqrt{n_{core}^2 - n_{cladding}^2}$$

half core thickness

free-space wavelength

$V < \frac{\pi}{2}$ - single-mode waveguide $V = \frac{\pi}{2}$ -TE_0 cut-off $V > \frac{\pi}{2}$ - multi-mode WG

$$V = const \rightarrow \Delta n \nearrow \; and \; a \searrow$$

Katsunari Okamoto, "Fundamentals of Optical Waveguides" 3rd edition, Academic Press, 2022
A. W. Snyder and J. D. Love, "Optical Waveguide Theory", Chapman & Hall, 1983

MODE STRUCTURE IN A WAVEGUIDE

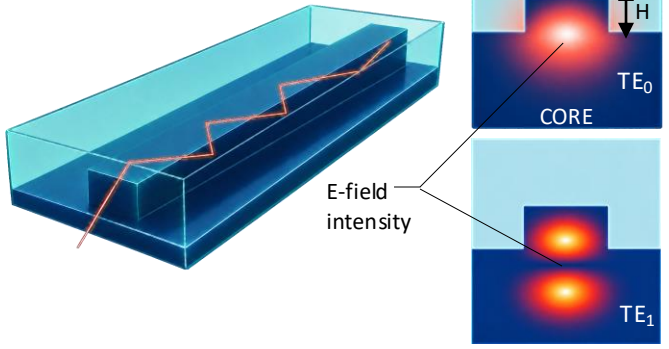

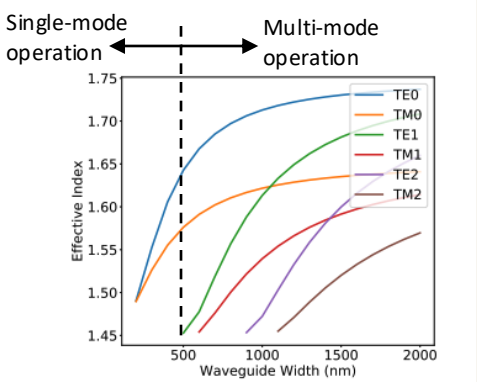

Martin Sinclair PhD Thesis, Univ. Glasgow

Qubit modal purity

Suppose the desired photon is $|\psi\rangle = |\psi\rangle_\omega |\psi\rangle_{pol} |\psi\rangle_{spatial}$

For a **single-mode waveguide**: $|\psi\rangle_{spatial,SM} = |\psi\rangle_{TE_0}$

For two photons traveling the same single-mode waveguide in the quantum circuit: $\langle |\psi\rangle_{TE_0} | |\psi\rangle_{TE_0} \rangle = 1$

For a photon in a **multimode waveguide:** $|\psi\rangle_{Spatial,MM} = \mathrm{a}|\psi\rangle_{TE_0} + \mathrm{b}|\psi\rangle_{TE_1}$

For two photons traveling the same MM waveguide in the quantum circuit can have different modal composition: $\langle |\psi\rangle_{Spatial,MM} | |\psi\rangle_{Spatial,MM} \rangle \neq 1$

If there is a multimode spatial component, indistinguishability gets lower

Suppose two photons enter the 50:50 beam splitter:

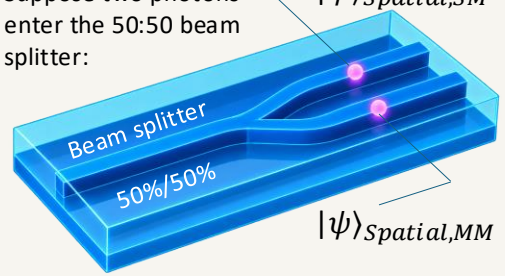

$|\psi\rangle_{Spatial,SM} = |\psi\rangle_{TE_0}$

$|\psi\rangle_{Spatial,MM} = \sqrt{1-\epsilon}|\psi\rangle_{TE_0} + \sqrt{\epsilon}|\psi\rangle_{TE_1}$

$M = 1 - \epsilon$

Partial indistinguishability

Optical phase vs quantum phase

Amplitude, Bloch-sphere rotation angle

$$|\psi\rangle = cos\frac{\theta}{2}|0\rangle + e^{i\phi}sin\frac{\theta}{2}|1\rangle$$

relative phase

DIRECTIONAL COUPLER (DC)

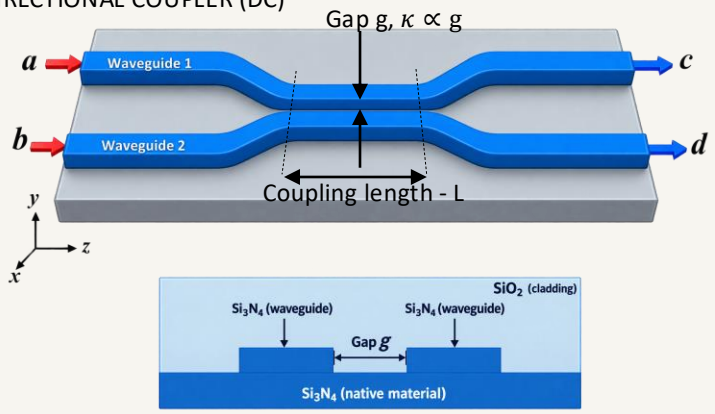

Directional coupler controls amplitude splitting and introduces a fixed phase

For identical waveguides: transfer matrix

$$\begin{pmatrix} c \\ d \end{pmatrix} = UD_C \begin{pmatrix} a \\ b \end{pmatrix}, U_{DC} = \begin{pmatrix} \cos(\gamma) & -isin(\gamma) \\ -isin(\gamma) & \cos(\gamma) \end{pmatrix}$$

Coupler mixing angle $\gamma = \kappa L$

$$\begin{pmatrix} a=1 \\ b=0 \end{pmatrix} \rightarrow \begin{pmatrix} \cos(\gamma) \\ -isin(y) \end{pmatrix} \rightarrow Pu_{pper} = T = \cos^2(\kappa L), Plo_{wer} = R = \sin^2(\kappa L)$$

$\gamma = \kappa L = \frac{\pi}{4} \rightarrow \frac{50\%}{50\%}$ beam splitter

$$\theta = 2\gamma = 2\kappa L \rightarrow \gamma = \frac{\pi}{4} \rightarrow \theta = \frac{\pi}{2}$$

$$|\psi\rangle = |0\rangle \rightarrow |\psi\rangle = \cos(\gamma)|0\rangle - isin(\gamma)|1\rangle = \frac{1}{\sqrt{2}}(|0\rangle - i|1\rangle)$$

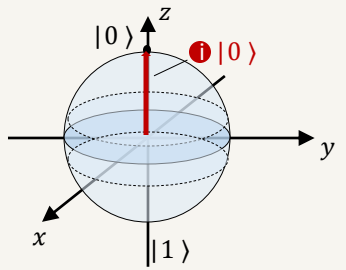

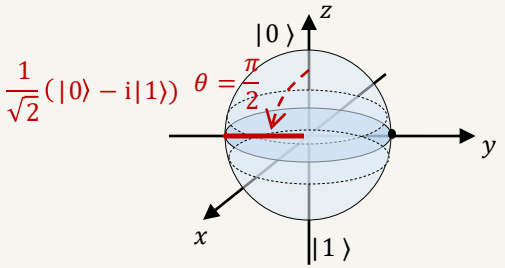

$\frac{1}{\sqrt{2}}(|0\rangle - i|1\rangle)$

PHASE SHIFTER

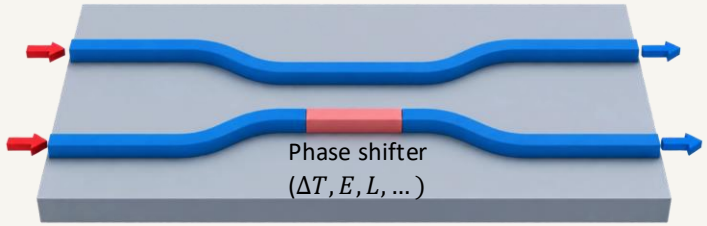

Phase shifter controls the relative phase

A mode propagating through a waveguide accumulates the optical phase:

$$\varphi_{opt} = \beta L = \frac{2\pi}{\lambda} n_{eff} L$$

The optical phase difference between two paths becomes the quantum relative phase :

$$\varphi_{upper} = \beta_u L_u \qquad \varphi_{lower} = \beta_l L_l \qquad \Delta\varphi = \varphi_{lower} - \varphi_{upper} = \frac{2\pi}{\lambda}(n_{eff,l} L_l - n_{eff,u} L_u)$$

Typ. $L_l = L_l = L \rightarrow \Delta\varphi = \frac{2\pi}{\lambda}\Delta n_{eff} L$

Thermo-optic phase shifter: $\Delta n_{eff}(T) \approx \frac{dn_{eff}}{dT}\Delta T$

Electro-optic phase shifter: $\Delta n_{eff}(E) \approx VL$

$$|\psi\rangle = \frac{1}{\sqrt{2}}(|0\rangle - i|1\rangle) \rightarrow |\psi\rangle = \frac{1}{\sqrt{2}}(|0\rangle - ie^{i\Delta\varphi}|1\rangle)$$

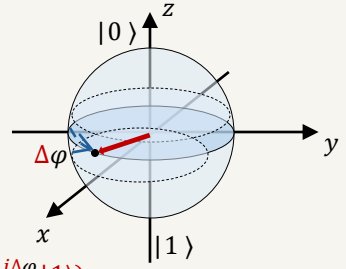

$\frac{1}{\sqrt{2}}(|0\rangle - ie^{i\Delta\varphi}|1\rangle)$

Mach-Zehnder interferometer (photonic single qubit gate)

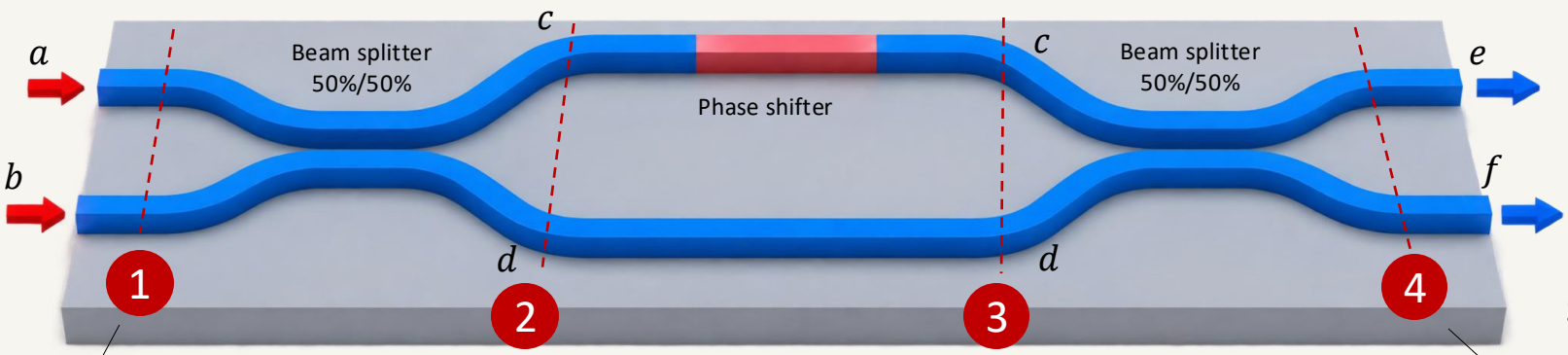

Detector counts N_e, $P_e = \frac{N_e}{N_e+N_f}$

Detector counts N_f, $P_f = \frac{N_f}{N_e+N_f}$

$$|\psi\rangle_{in} = |a = 1, b = 0\rangle$$

One photon in the mode a

Vacuum in the mode b

$$|\psi\rangle_{out1} = U_{DC1}|\psi\rangle_{in}$$

$$|\psi\rangle_{out1} = \frac{|c\rangle - i|d\rangle}{\sqrt{2}}$$

- Equal amplitudes
- Phase shift : $\varphi = -\frac{\pi}{2}$

$$|\psi\rangle_{out2} = U_{\Delta\varphi}|\psi\rangle_{out1}$$

$$|\psi\rangle_{out2} = \frac{|c\rangle - ie^{i\Delta\varphi}|d\rangle}{\sqrt{2}}$$

Limiting cases:

1) $\Delta\varphi = 0 \rightarrow |\psi\rangle_{out2} = \frac{|c\rangle - i|d\rangle}{\sqrt{2}} \rightarrow P_e = 0, P_f = 1$
2) $\Delta\varphi = \pi \rightarrow |\psi\rangle_{out2} \frac{|c\rangle + i|d\rangle}{\sqrt{2}} \rightarrow P_e = 1, P_f = 0$
3) $\Delta\varphi = \pi/2 \rightarrow P_e = 1/2, P_f = 1/2$

Second directional coupler converts relative phase into measurable output probabilities

$$|\psi\rangle_{out3} = U_{DC2}|\psi\rangle_{out2}$$

$$|c\rangle \rightarrow \frac{|e\rangle - i|f\rangle}{\sqrt{2}} \qquad |d\rangle \rightarrow \frac{-i|e\rangle + |f\rangle}{\sqrt{2}}$$

$$|\psi\rangle_{out3} = \frac{1}{\sqrt{2}}\left(\frac{|e\rangle - i|f\rangle}{\sqrt{2}} + ie^{i\Delta\varphi}\frac{-i|e\rangle + |f\rangle}{\sqrt{2}}\right)$$

$$|\psi\rangle_{out3} = A_e|e\rangle + A_f|f\rangle \qquad A_e = \frac{1 - e^{i\Delta\varphi}}{2} \qquad A_f = -\frac{(1 + e^{i\Delta\varphi})}{2}$$

$$1 + e^{i\Delta\varphi} = 2e^{i\Delta\varphi/2}\cos(\Delta\varphi/2) \qquad 1 - e^{i\Delta\varphi} = -2ie^{i\Delta\varphi/2}\sin(\Delta\varphi/2)$$

$$P_e = |A_e|^2 = sin^2(\Delta\varphi/2)$$

$$P_f = |A_f|^2 = cos^2(\Delta\varphi/2)$$

Nielsen and Chuang *Quantum Computation and Quantum Information* Cambridge University Press (2010 edition)
A. Politi, et al., *Silica-on-silicon waveguide quantum circuits* *Science* 320, 646–649 (2008)
W. R. Clements, et al. *Optimal design for universal multiport interferometers* *Optica* 3, 1460–1465 (2016).

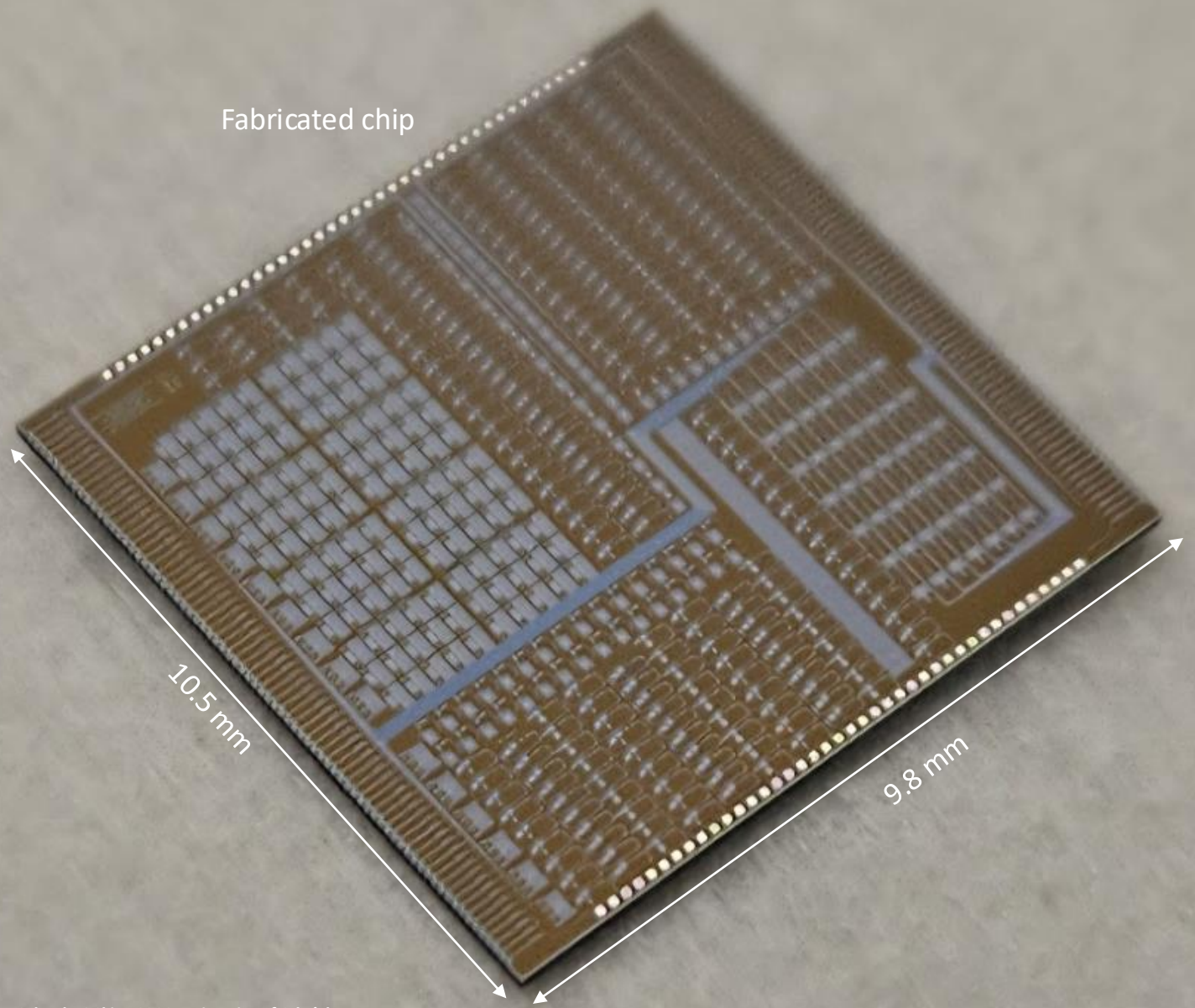

From material processing to a real device

From material and processing to a real device performance

HBT section with grating couplers

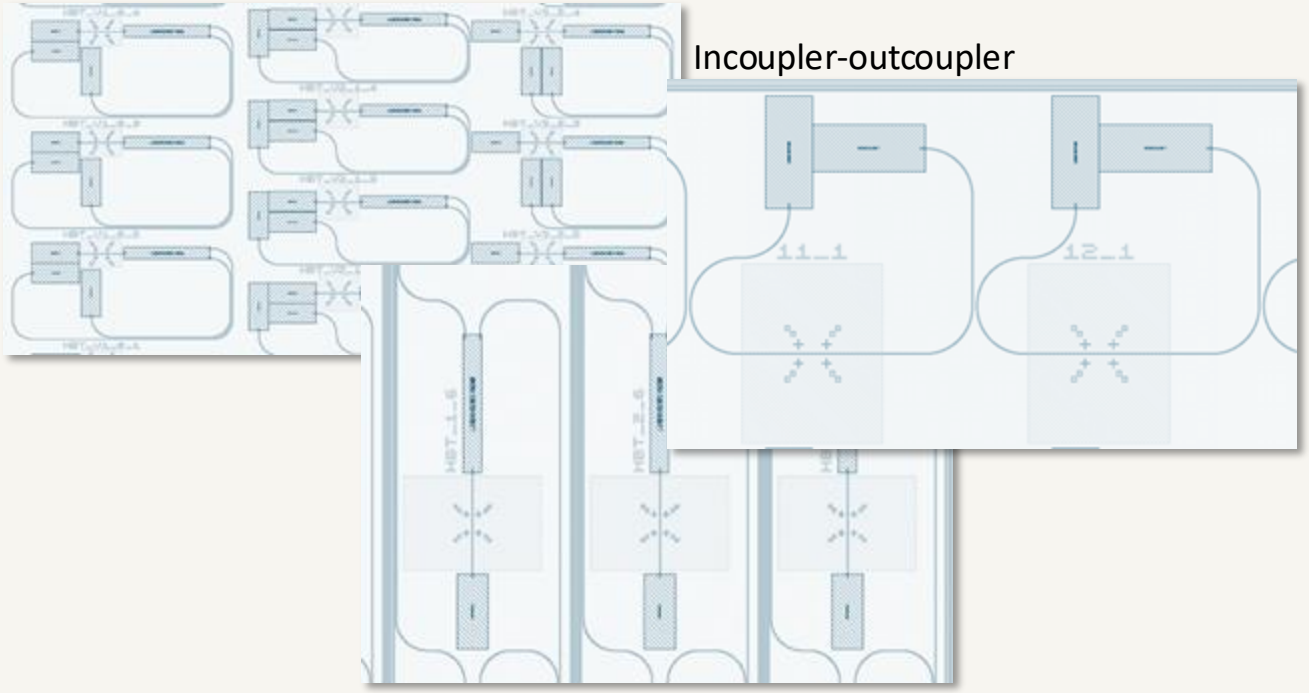

SiO_2/SiN/Si chip technology

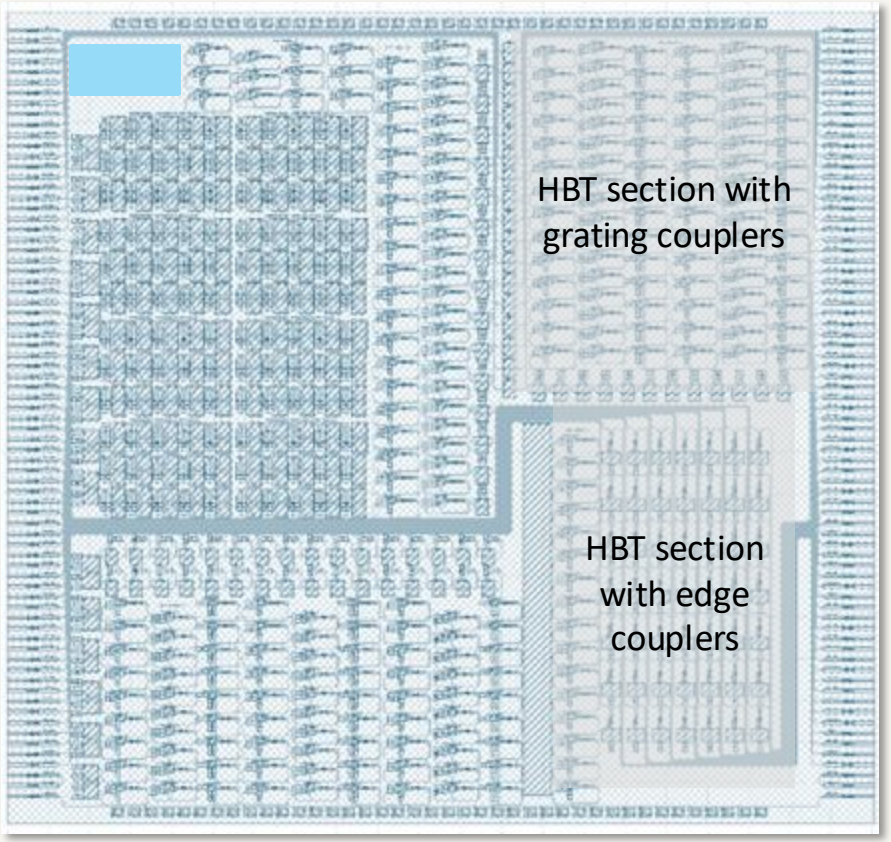

Chip size: 9.8 mm x 10.5 mm

PART IV

Single photon source – self-assembled semiconductor quantum dot

How can a nanoscale emitter produce one telecom photon at a time?

Quantm computation and telecommunication in the fiber-network infrastracture

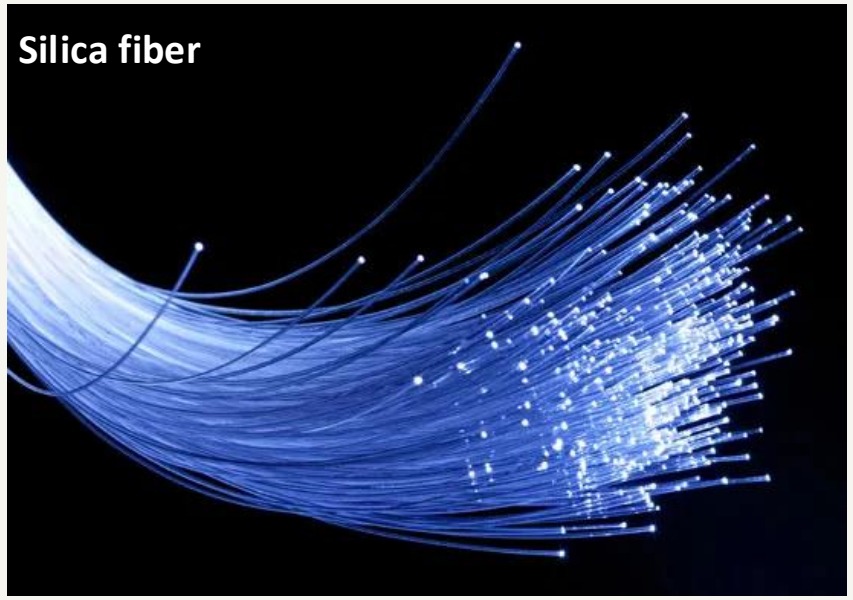

Attenuation of transmitted light in a silica fiber

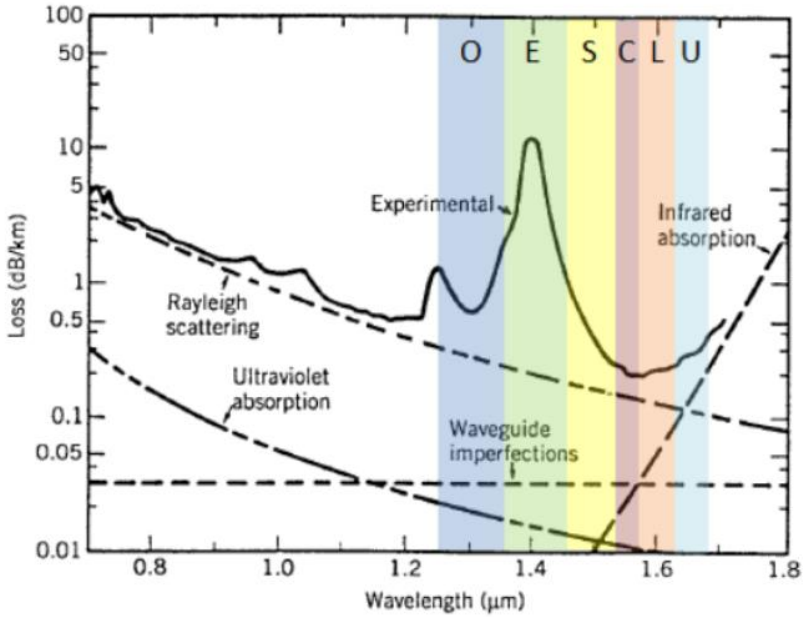

O band: "Original", 1260 – 1360nm
E band: "Extended", 1360 – 1460nm
S band: "Short", 1460 – 1530nm
C band: "Conventional", 1530 – 1565nm ← The lowest losses
L band: "Long", 1565 – 1625nm
U band: "Ultra-long", 1625 – 1675nm

Luiz anet Neto, PhD Thesis, IMT Atlantique

Single photon emitters at 1550 nm

Heralded photon pairs generation

- spontaneous parametric down-conversion – SPDC;
- spontaneous four-wave mixing - SFWM;

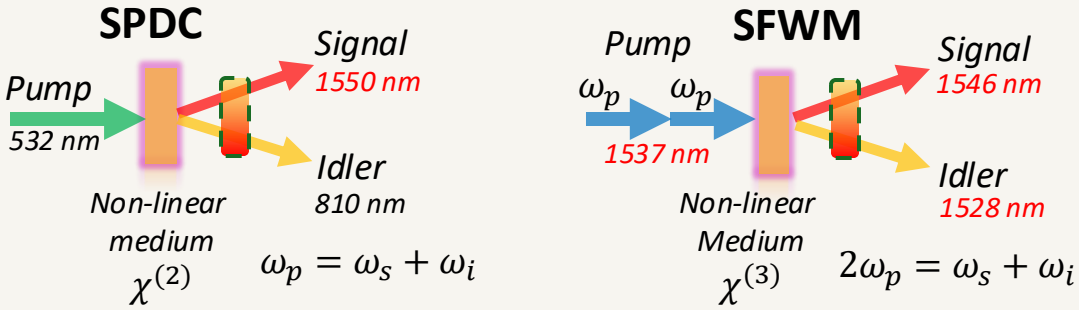

Pros: @300 K
Cons: Pobabilistic, ~~on-demand~~, low SPS emission rate

S. Fasel, et al. New J. Phys. 6 163 (**2004**);
O. Alibart, et al. Opt. Lett. 30 1539 (**2005**);
A. Soujaeff, et al. J. Mod. Optics 54, 467 (**2013**);

A. Valles, et al. Opt. Express 21, 10841(**2013**);
M. Fiorentino, et al., IEEE Phot. Technol. Lett. 14, 983(**2002**);
K. Inoue and K. Shimizu Jpn. J. Appl. Phys. 43, 8048(**2004**);

Aryl sp^3 defect in carbon nanotubes

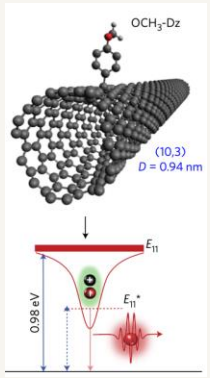

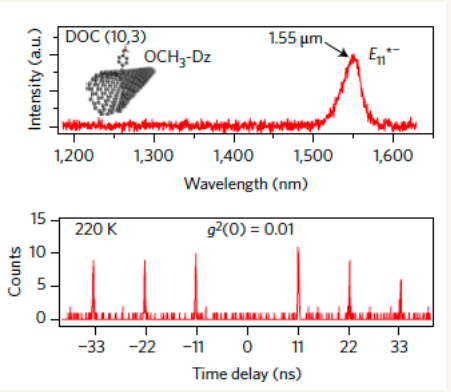

X. He, et al., Nat. Photonics 11, 577(**2017**).

Pros: Low g^2 at high T
Cons: Broad emission line, Implementation

Erbium ions (Er^{3+})

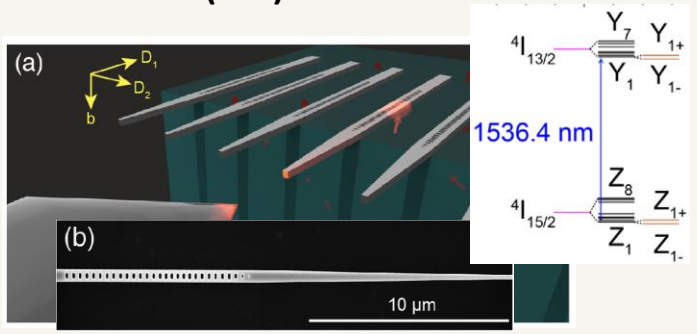

Pros: @300 K, long lifetime (quantum repeater)
Cons: spectral wandering, low SPS emission rate

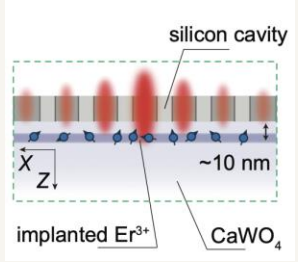

A. M. Dibos, et al. Phys. Rev. Lett. 120, 243601(**2018**); S. Ourari, et al. arXiv:2301.03564v1 (**2023**)

Defects in bulk $MoTe_2$

Pros: TMDC material
Cons: Broad emission line, Implementation

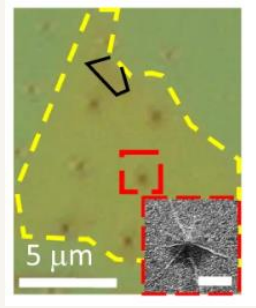

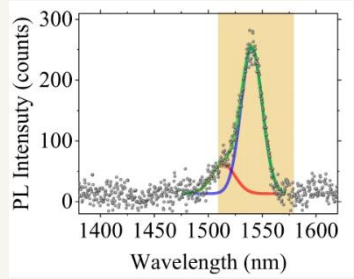

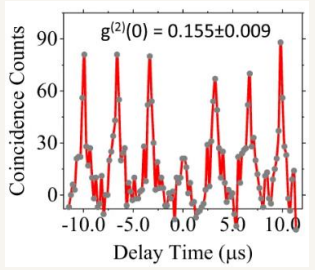

H. Zhao, et al., Nat Commun. 12, 6753 (**2021**).

Semiconductor quantum dot

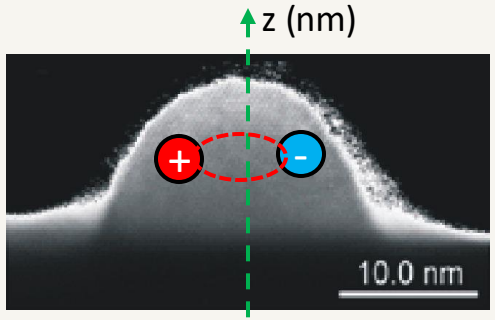

P. Michler (Ed.), *Single Semiconductor Quantum Dots*, NanoScience and Technology, Springer, Berlin/Heidelberg, 2009

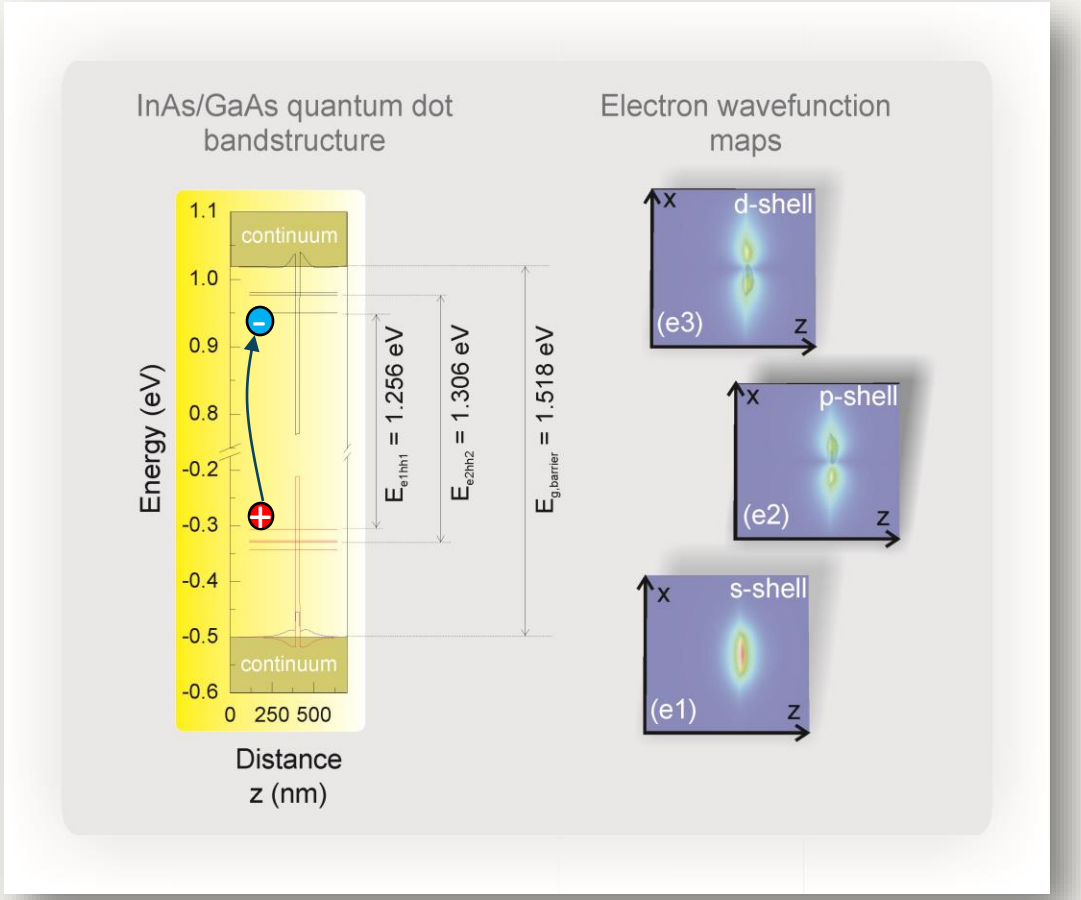

Dr Janusz Andrzejewski, PWr,
QD bandstructure, kp framework

Two-particle picture

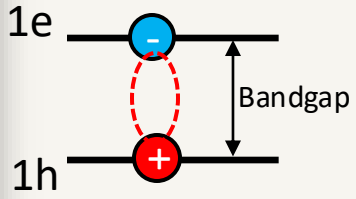

Single-particle picture

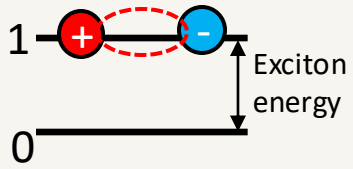

Exciton = Coulomb bound electron-hole pair

Exciton energy = Bandgap – Coulomb binding energy

Coulomb binding energy ~ 15 - 50 meV

Semiconductor quantum dot

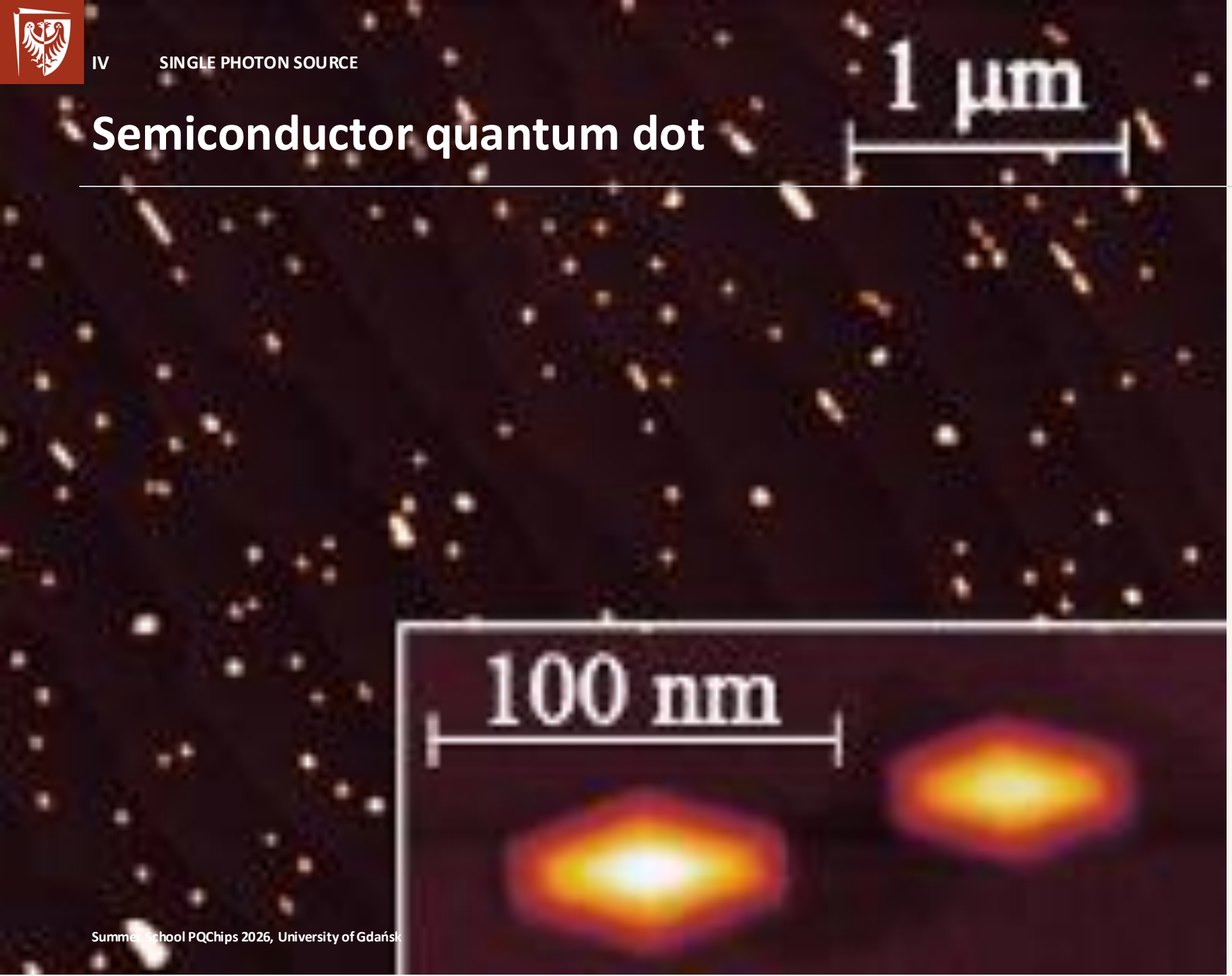

InAs/InP self-assembled quantum dots

Geometry of InAs/InP quantum dots

AFM image, surface QDs

HR-STEM image

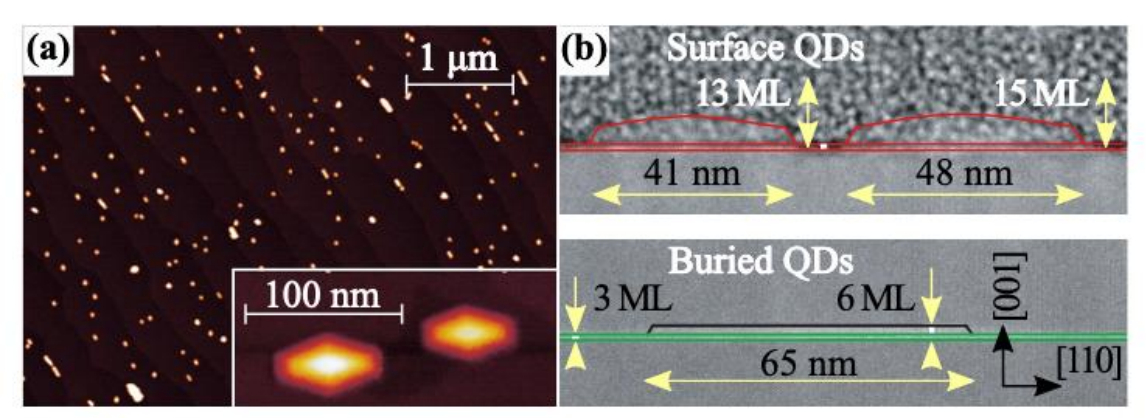

QD size statistics

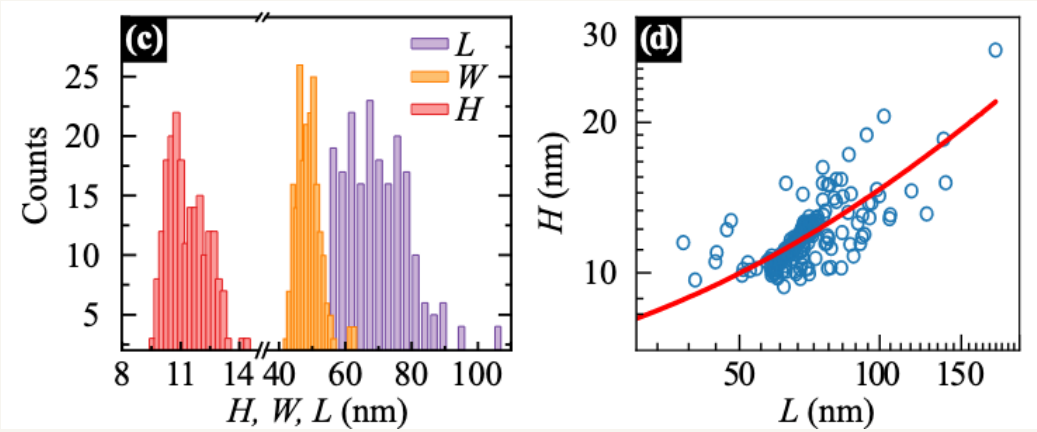

QD geometry

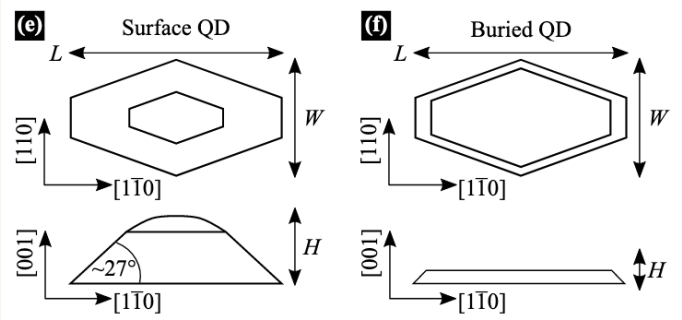

Main features of SK QDs:

- QD surface density: 10^7-10^9 cm^{-2} ;
- Emission wavelength: 1250 nm - 1800 nm
- QD geometry: in-plain anisotropy;

Self-assembled InAs/InP quantum dot – the growth process

Metalorganic Vapour Phase Epitaxy - MOVPE

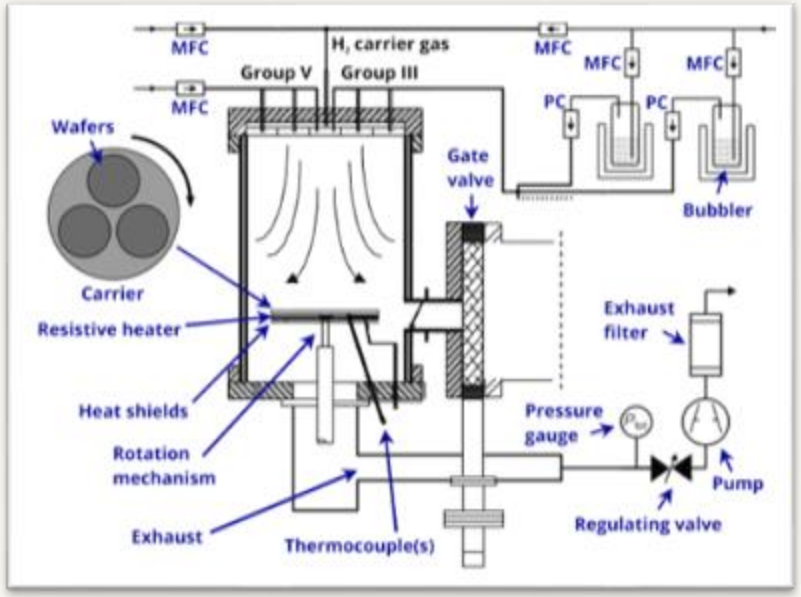

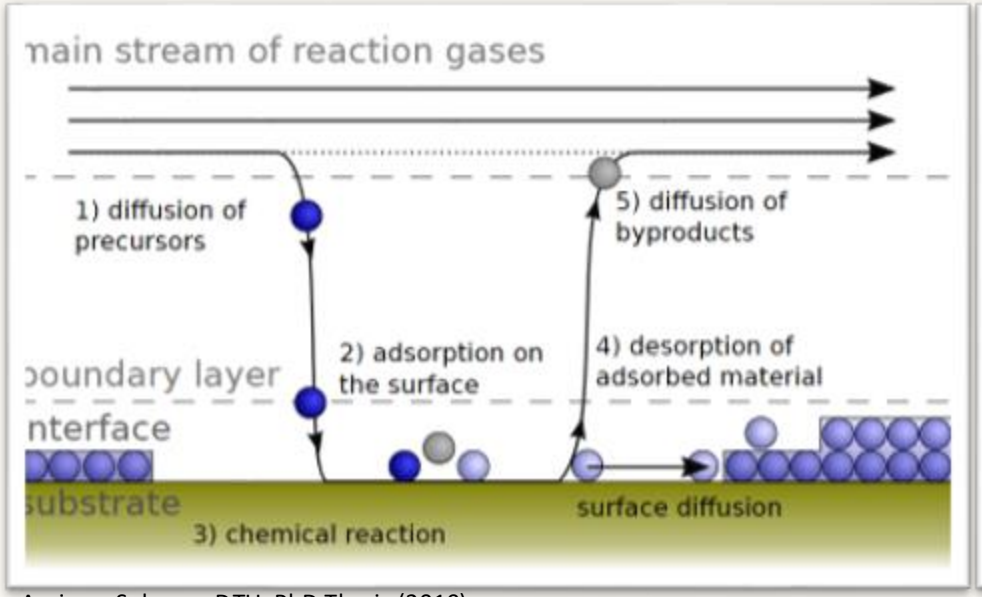

Aurimas Sakanas, DTU, PhD Thesis (2019)

Growth precursors

- phosphine **PH_3**
- arsine **AsH_3**
- trimethylindium **TMIn**

Growth controlling parameters

- QDs growth temperature (T_g)
- TMIn flow rate (III/V ratio)
- QDs growth time (t_g)
- PH_3/AsH_3 flow rates (P/V ratio)

Self-assembled InAs/InP quantum dot – the growth process

QD formation – self-assembled process

Stranski-Krastanow (SK)

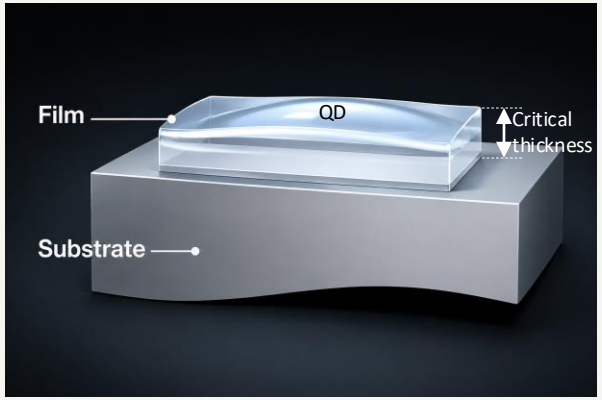

The method is based on strain relaxation, which occurs between two lattice-incompatible materials

The lattice constant difference between InAs and InP is ~3%

P. Holewa et al. Nature Communication 15, 3358 (**2024**)
Y. Berdnikov et al., Scientific Reports 14, 23697 (**2024**)
P. Holewa, et al. ACS Photonics 9, 7, 2273 (**2022**) – **SK QDs**
P. Holewa et al. Phys. Rev. B 101, 195304 (**2020**) – **SK QDs**
P. Holewa et al. Nanophotonics 11, 1515 (**2022**) – **DE QDs**

Droplet epitaxy (DE)

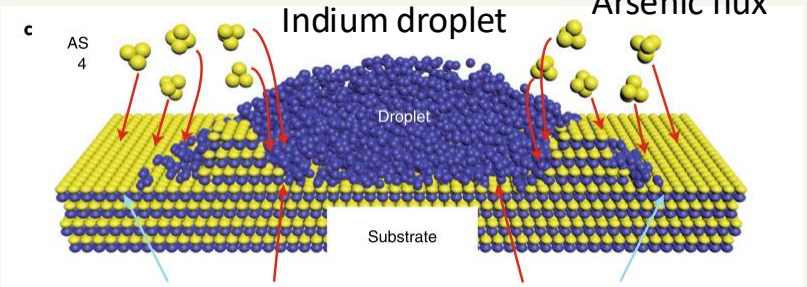

M. Gurioli, *Nat. Mater.* **18**, 799 (2019).

Separated supply of elements – more parameters to tune then in SK, mainly:

- growth temperaturę;
- amount of indium;

P. Holewa et al. Nanophotonics 11, 1515 (**2022**) – **DE QDs**

Size of a quantum dot defines emission energy

Ensemble emission for SK QDs

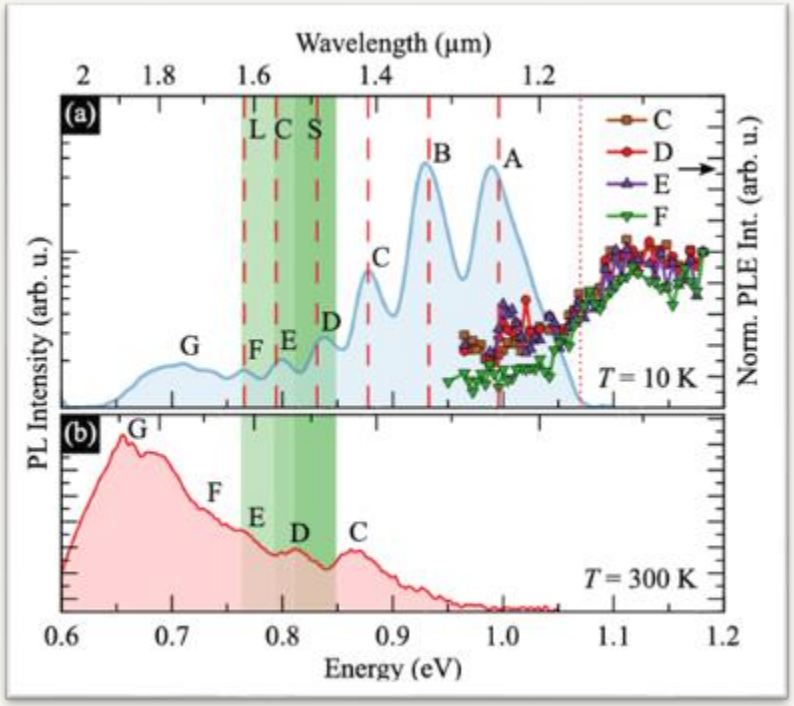

Ensemble emission for DE QDs

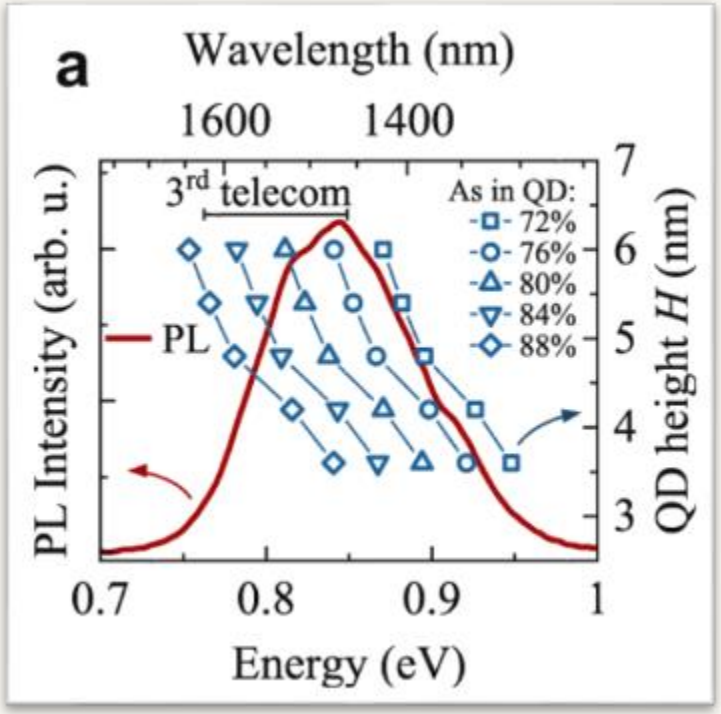

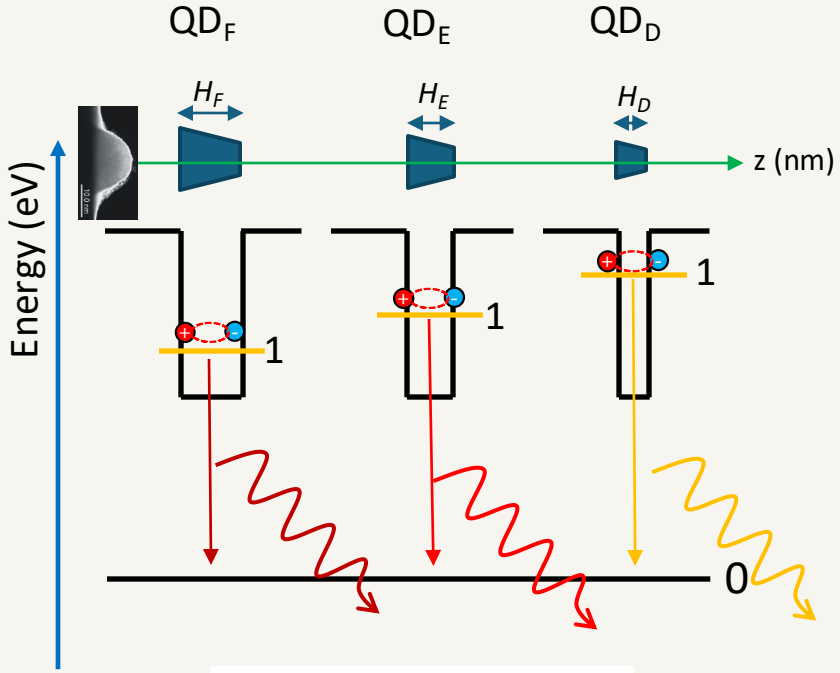

$$E(H,L) \simeq \sum_{ij} a_{ij} H^{-i} L^{-j}$$

QDs ensemble emission span a broad photon energy range: 1300-1700 nm

Single photon generators in a quantum dot

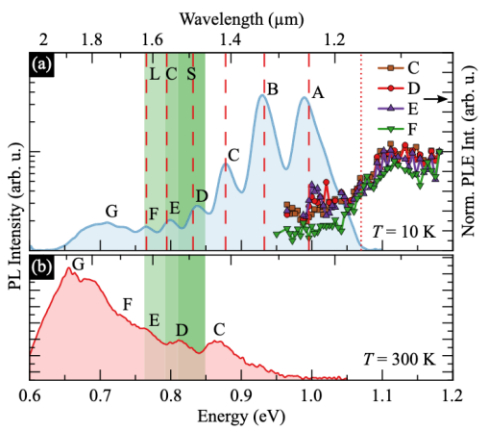

Isolation of few emitters emission

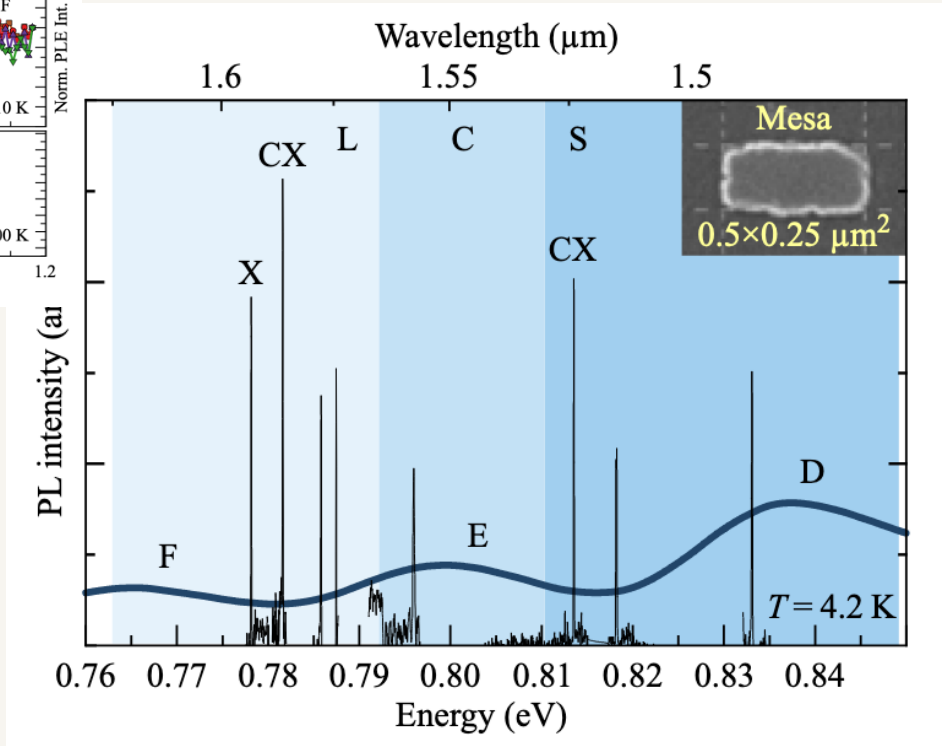

A variety of excitonic complexes able to recombine in a QD

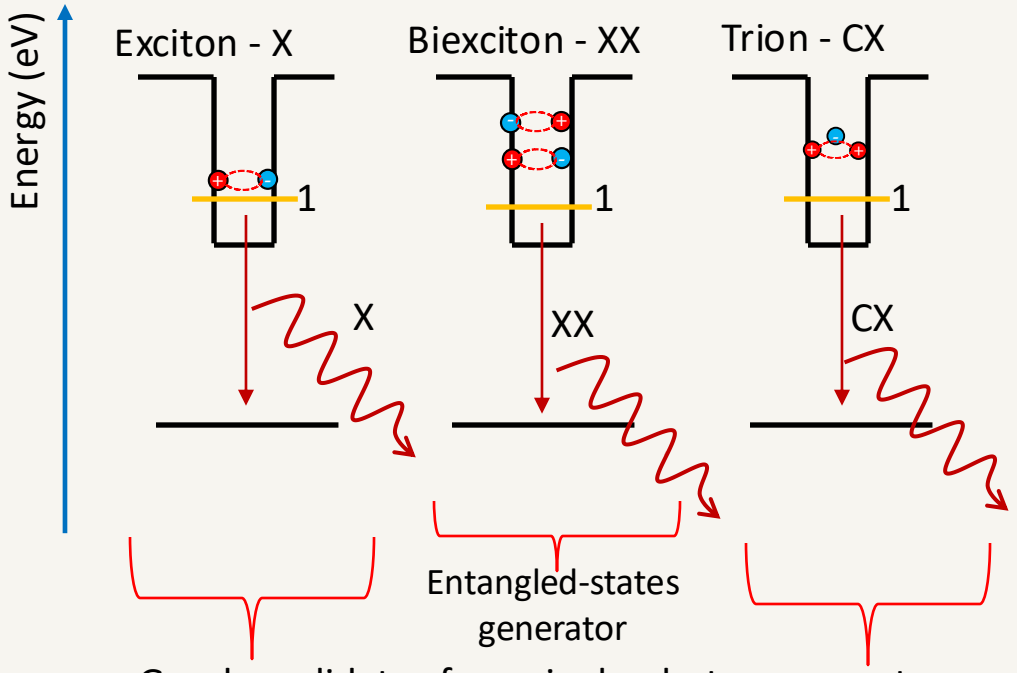

Various emission complexes can be associated to a single QD emitter, it is important to identify them and filter out the photon states generator of desired parameters (having X, XX, or CX emission in the specified spectral range)

Requirements for a (QD-based) single photon source

Key parameter

- High-brightness/photon extraction efficiency (η)
- High photon generation rate (G)
- On-demand operation
- High single photon generation purity
- High photon indistinguishability
- Deterministic fabrication

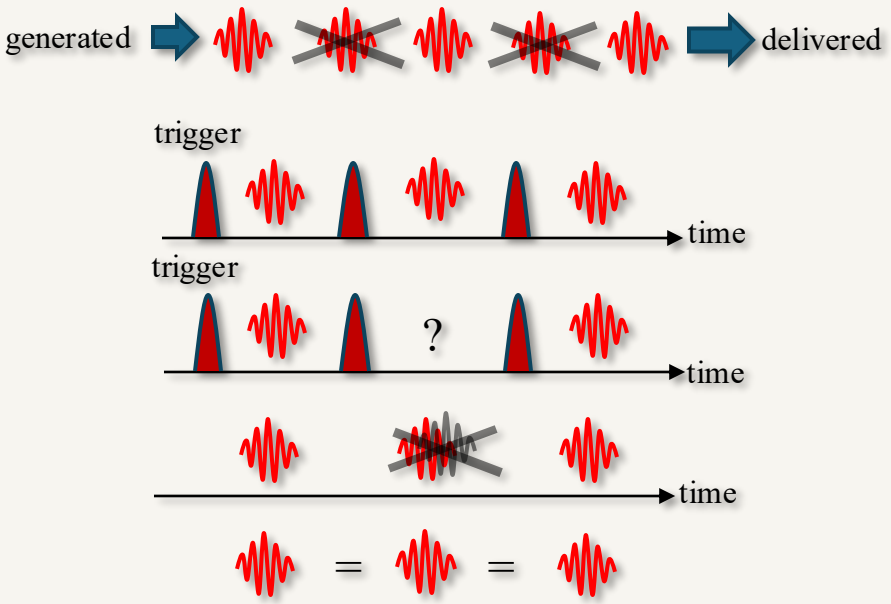

S. Buckley, K. Rivoire, J, Vučković, Rep Prog. Phys. 75, 126503 (**2012**)
P. Senellart, G. Solomon, A. White Nat. Nanotechnol. 12, 1026 (**2017**)
P. Holewa and M. Syperek, Nat. Nanotechnol. 21, 618 (**2026**)

Expected performance

- η >90%
- G~1-2 GHz (0.5-1 ns)
- Trigger pulse → single photon
- >99% purity → $g^2(\tau=0) < 1\times10^{-2}$
- >98% purity → TPI Visibility V>98%
- The device processing yield >>50%

Engineering photon extraction efficiency η_{ext} near 1550 nm

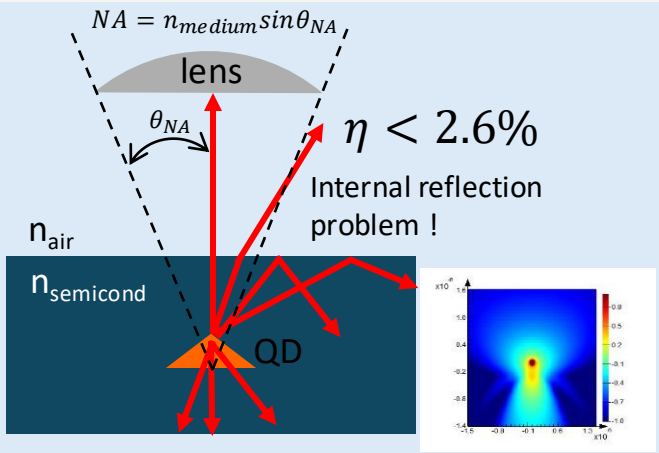

$$\eta_{ext}(NA) = \frac{photons\ at\ the\ first\ lens}{photons\ emitted\ by\ the\ QD}$$

@1550 nm:

$$n_{InP} \approx 3.17, n_{air} = 1$$

Critical angle θ_c :

$$\theta_c = sin^{-1}\left(\frac{n_{air}}{n_{InP}}\right) = sin^{-1}\left(\frac{1}{3.17}\right) \approx 18.4°$$

The fraction of the isotropic emission hitting the upper hemisphere:

$$\eta_{ext}(NA = 1) = \frac{1 - cos\theta_c}{2} \approx \frac{1 - \cos(18.4°)}{2} \approx 0.0255$$

$$\eta_{ext}(NA = 1) = 2.55\%$$

$$\eta_{ext}(NA = 0.4) \approx \frac{1 - \cos(26.4°)}{2} \approx 0.4\%$$

Dielectric confinement enforcing light coupling to the fundamental waveguide mode

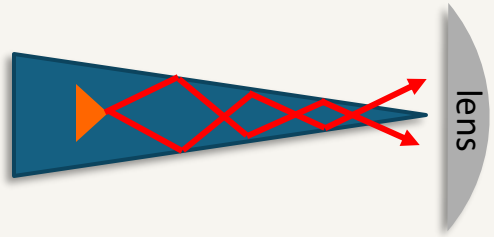

Optical horn structure

$\eta \approx 11\%, NA = 055$

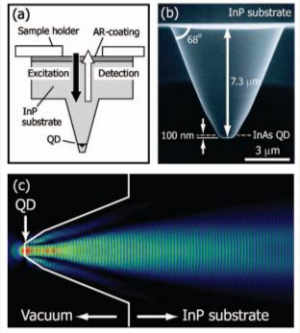

K. Takemoto, et al. J. Appl. Phys., 101, 081720 (**2007**)

"weak" cavity – MBE DBR (InGaAlAs/InP)/QD/air

$\eta \approx 13.3\%, NA = 0.4$

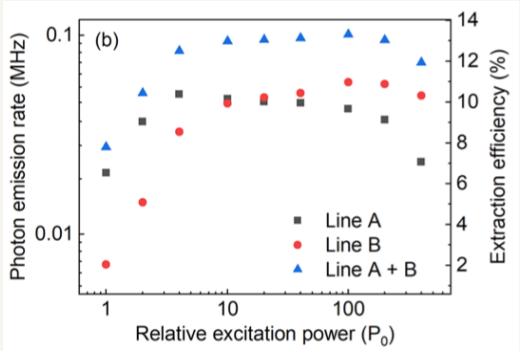

A. Musiał, et al. Appl. Phys. Lett. 118, 221101 (**2021**);

Dielectric confinement + cavity electrodynamics

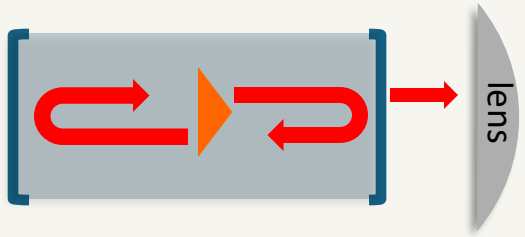

"weak"cavity – metal/QD/air (flip chip technology)

$\eta \approx 10\%, NA = 0.4$

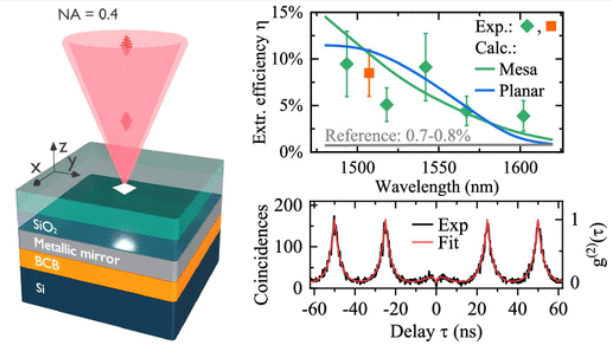

P. Holewa, et al. ACS Phot. 9, 7, 2273 (**2022**)

Towards better source performance – full cavity

Micropillar microcavity

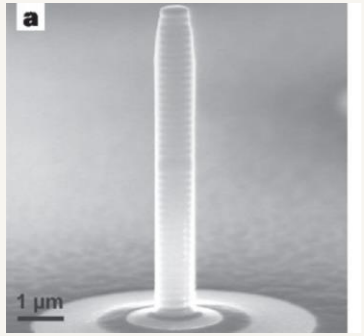

JP Reithmaier et al.,
Nature 432, 197-200 (**2004**)

Highly directional emission/out of plane
High extraction efficiency
High Purcell enhancement
Highly critical dipole-cavity mode matching

Microdisk microcavity

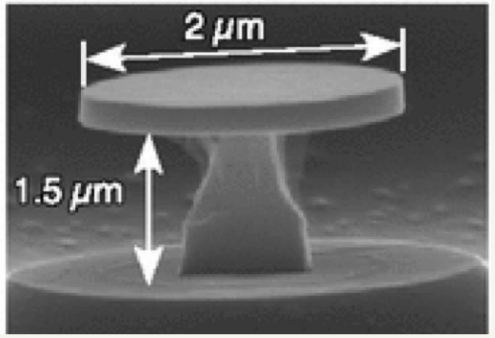

E. Peter et al.,
Phys. Rev. Lett 95, 067401 (**2004**)

High Purcell enhancement

Mechanically unstable

Radial emission

Photonic Crystal (PhC) uCavity

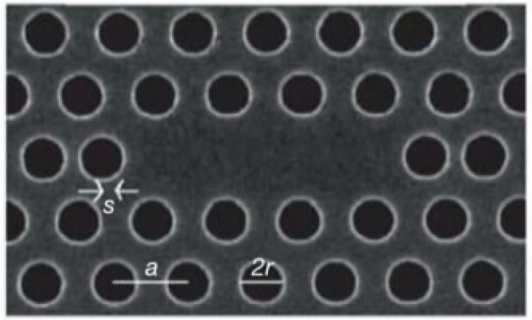

T. Yoshie et al., Nature 432, 2000 (**2004**)

Highly directional in-plane emission (on-chip photonics)

First demonstration of cavity-coupled-InAs/InP QD at 1550 nm

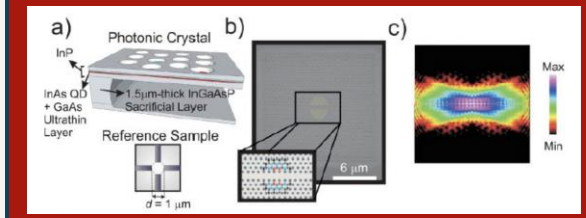

M. D. Birowosuto, et al. Sci. Rep. 2, 321 (**2012**)

Circular Bragg Grating (CBG) microcavity

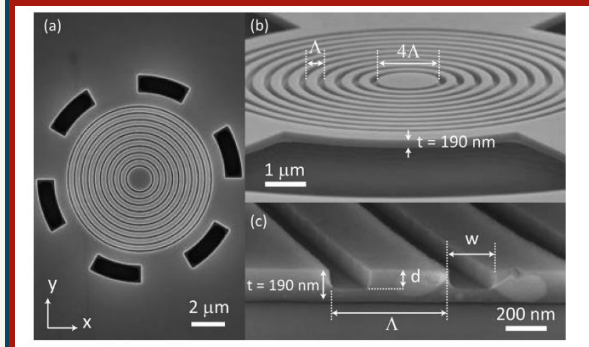

M. Davanço et al., Appl. Phys. Lett. **99**, 1 (**2011**).

Highly directional emission/out of plane
High extraction efficiency

High Purcell enhancement

Relaxed dipole-cavity mode matching

Purcell efect

Spontaneous emission is therefore determined not only by the emitter but also by its photonic environment.

$$\Gamma = \frac{2\pi}{\hbar^2}\left\langle \left| \left\langle \bar{d} \cdot E(\vec{r},t) \right\rangle \right|^2 \right\rangle \rho(\omega) = \frac{1}{\tau}$$

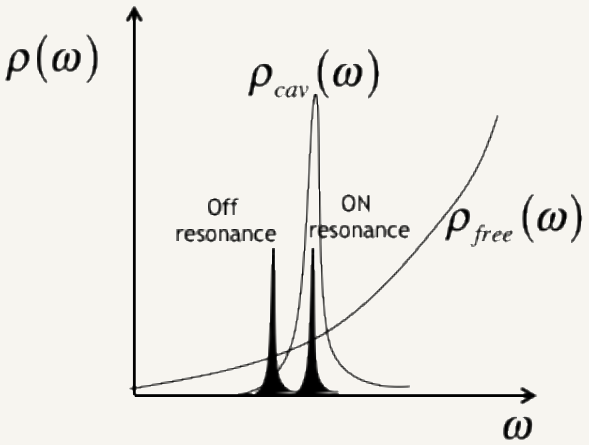

Cavity-modified photonic densit y of states

$$\rho_{cav}(\omega) = \frac{2}{\pi}\frac{\Delta\omega}{4(\omega-\omega_c)^2 + \Delta\omega_c^2}$$

The Purcell factor quantifies how strongly the photonic environment modifies an emitter's spontaneous emission rate.

Purcell effect (1946)

$$F_P = \frac{\Gamma_{cav}}{\Gamma_{free}} = \frac{\rho_{cav}}{\rho_{free}}$$

$$F_P = F_P^{max} \times \frac{\left|\bar{d}\bar{E}(\bar{r})\right|^2}{|\bar{d}|^2 |E_{max}|^2} \times \frac{1}{1 + 4(\omega-\omega_c)^2/\kappa^2}$$

$$F_P^{max} = \frac{3}{4\pi^2}\left(\frac{\lambda_c}{n}\right)^3 \frac{Q}{V}$$

Spatial and polarization overlap between emitter and the cavity mode

Spectral overlap between an emitter and the cavity mode

Q- quality factor of a cavity, λ_c- mode wavelength, n – effective refractive index of the cavity, V – cavity volume, ω_c- cavity mode frequency, $\kappa = \Delta\omega_c$- cavity resonance linewidth, $\bar{d}$- the transition electric dipole moment, $\bar{E}(\bar{r})$ – the cavity field

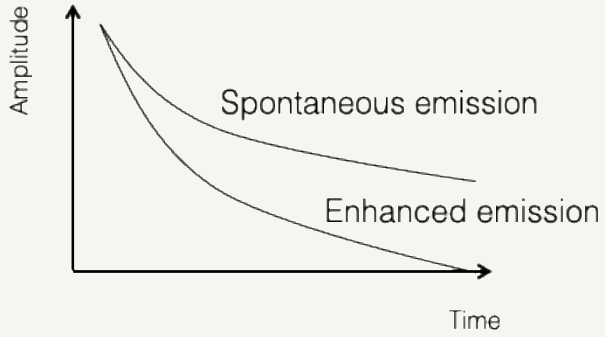

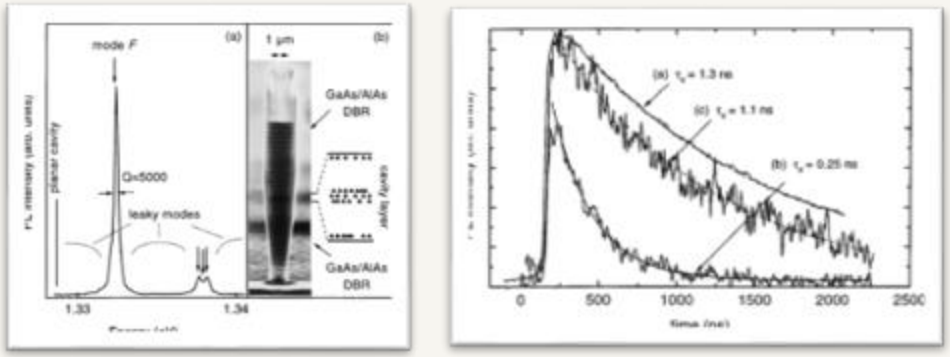

J. M. Gerard et al., Phys. Rev. Lett. 81, 1110 (1998)

Cavity performance

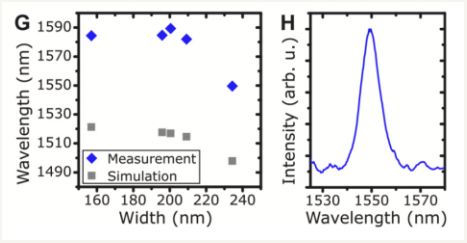

R. Sittig, et al., Nanophotonics 11(6), 1109 (**2022**)

C. Nawrath, et al., arXiv:2207.12898v1 (**2022**)

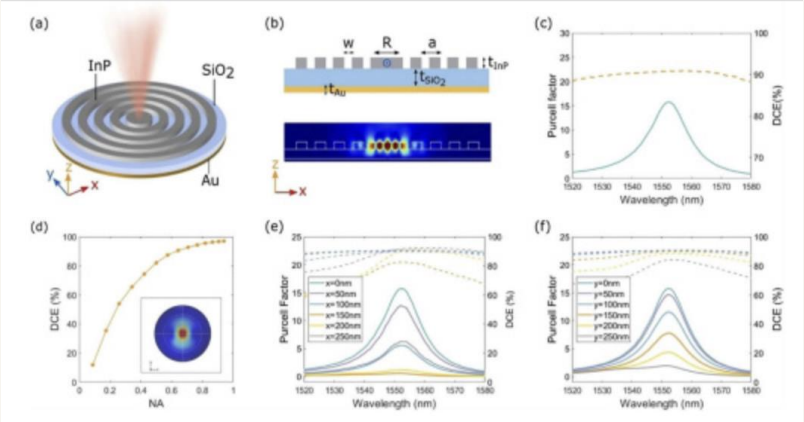

L. Barbiero, et al., Optics Express 30(7), 10919, (**2022**)

Calculated performance of a CBG cavity – comparison to a micropillar cavity

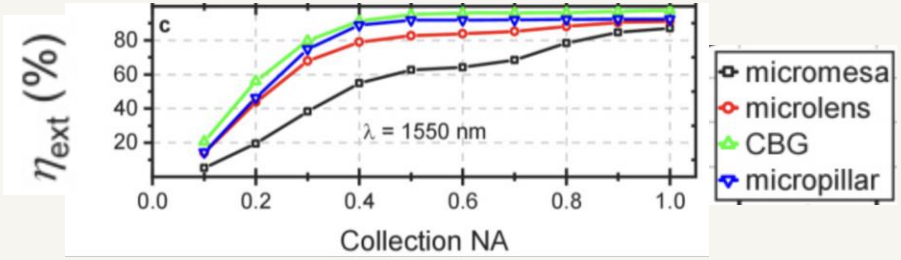

Cavity	Extraction efficiency	Purcell factor	Bandwidth (nm)
CBG	91.2% (NA=0.4)	43.3	3.3 nm
Micropillar	88.9% (NA=0.4)	9.7	0.3 nm

L. Bremer, et al., Optics Express 30(10), 15913, (**2022**)

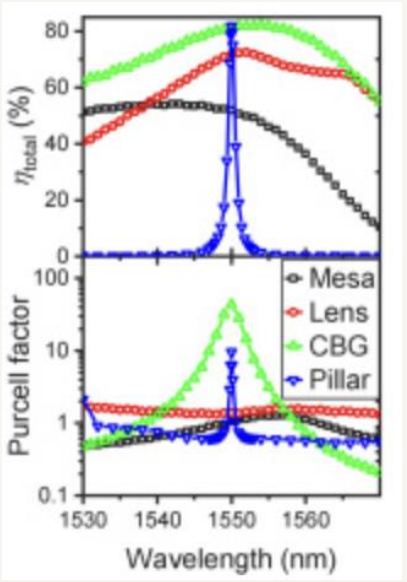

Best performance

- QD position at the cavity centre
- Wavelength matching between the cavity mode and QD emission

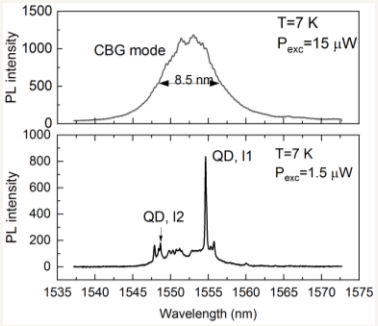

Localization of a quantum dot

Enhancement of η (7x)

SNR~12

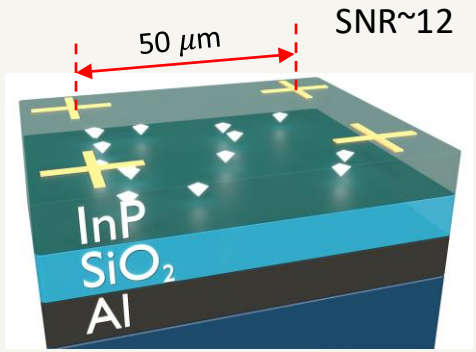

P. Holewa, et al. ACS Phot. 9(7), 2273 (**2022**)

Unprocessed image with QD-related spots

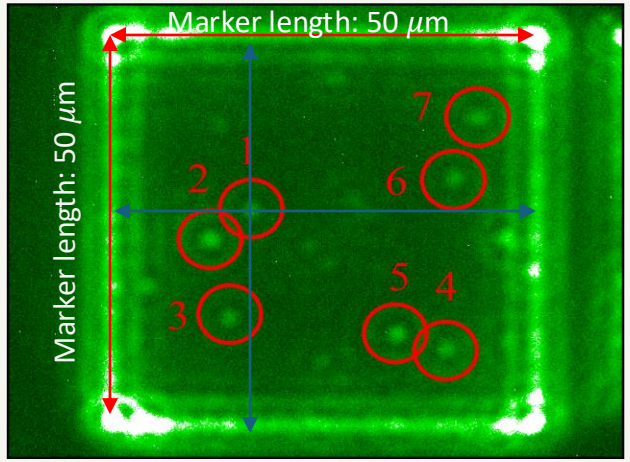

QD position accuracy (better than 90 nm)

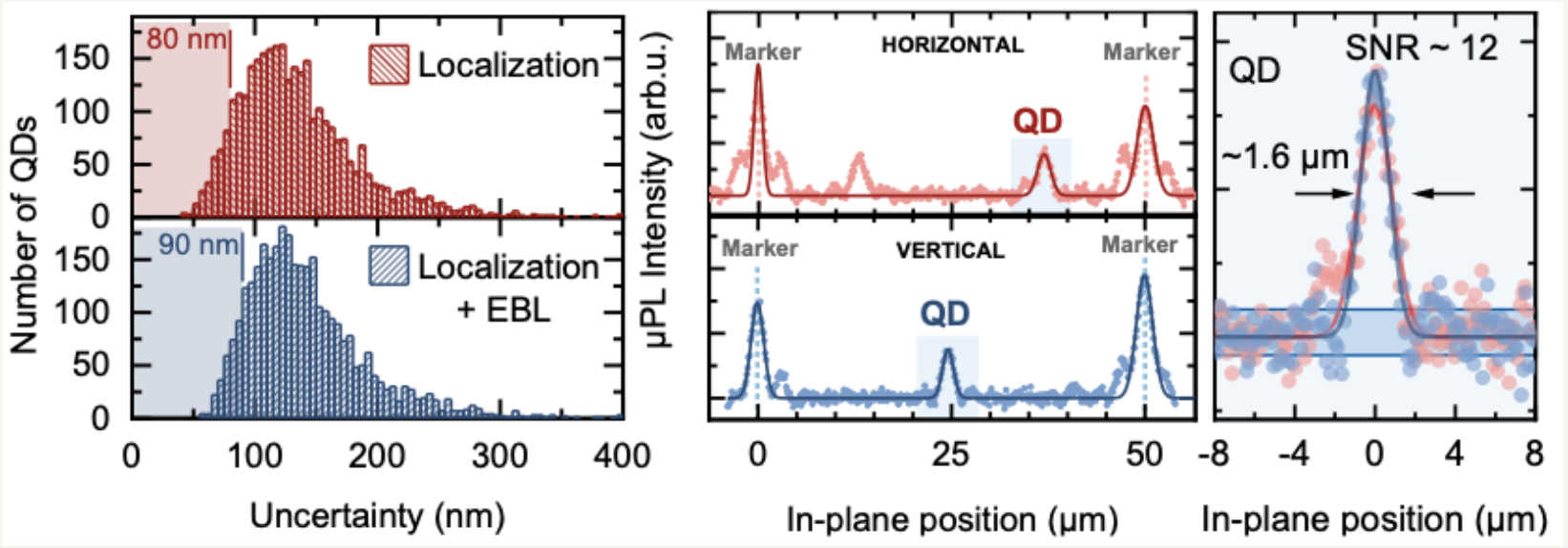

P. Holewa et al. Nature Communications 15, 3358 (**2024**)

Various cavity realizations

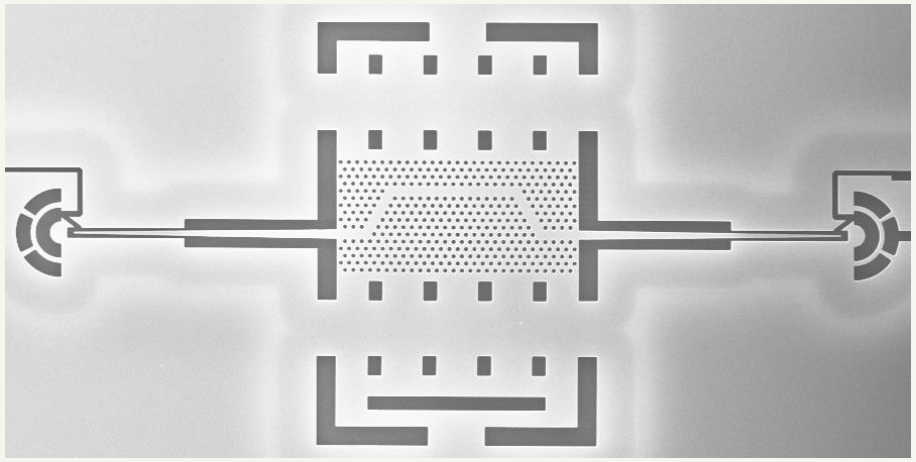

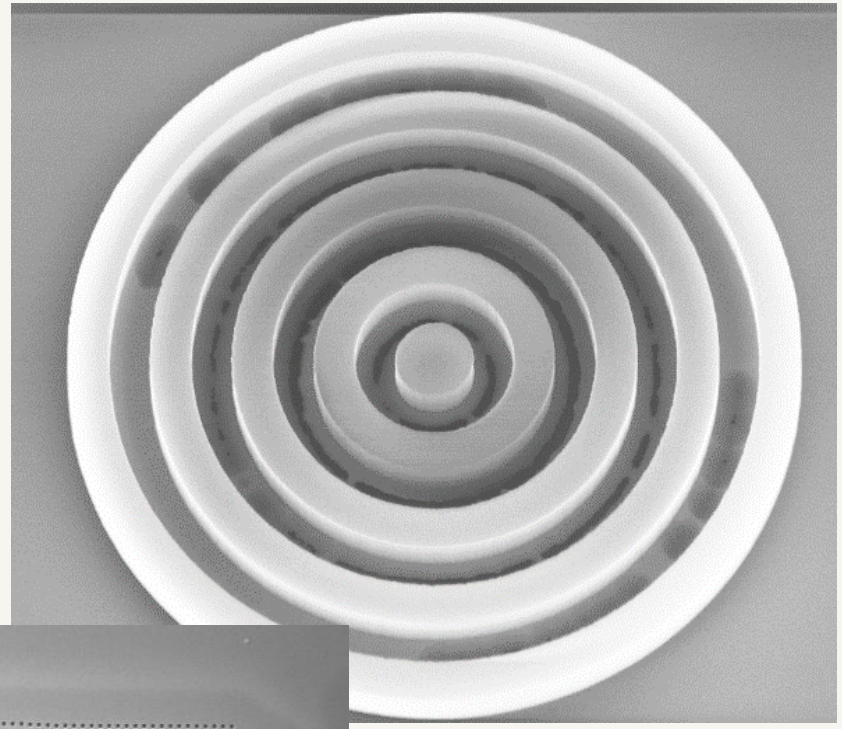

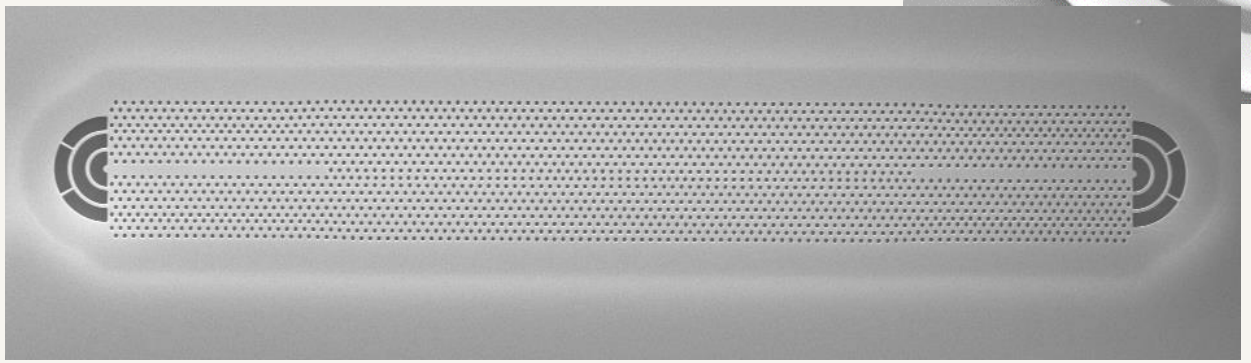

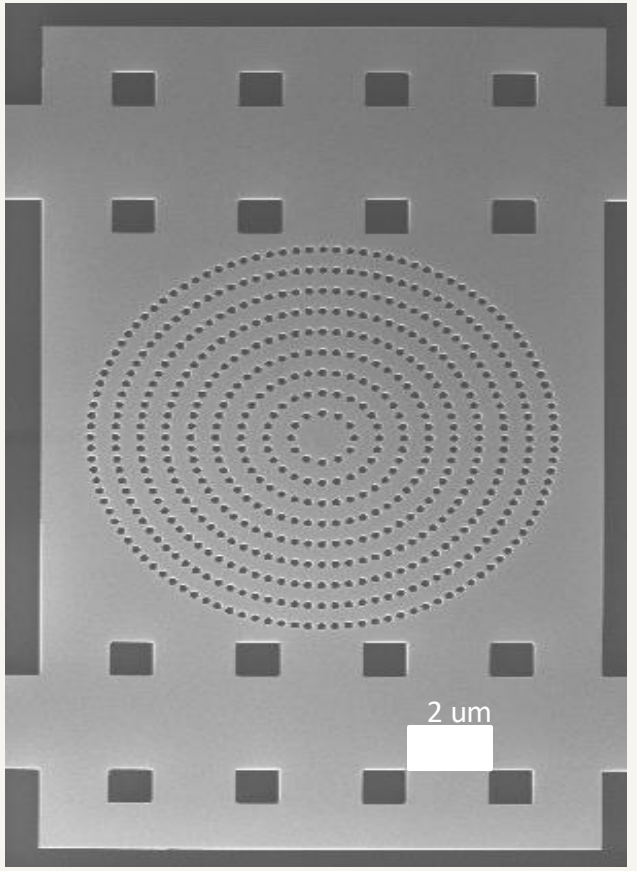

Moire cavity – an isolated flat band dispersion of photonic modes

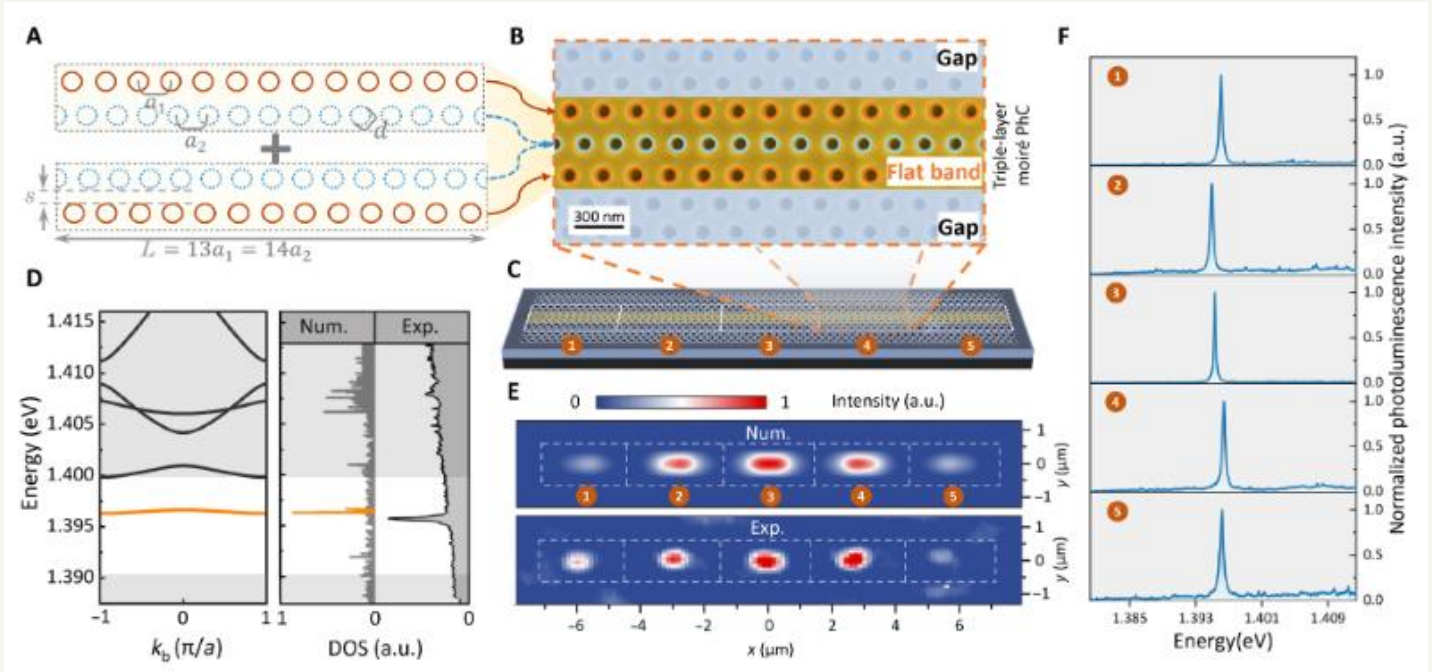

Yu-Tong Wang, …, Feng Liu „Moiré cavity quantum electrodynamics" Science Advances **11**, eadv8115 (2025)

For propagating photons in a „norma" situation one have:

$$\omega = \omega(k)$$

For a flat band situation, it is: $\omega(k) = constant$

Different photons have the same frequency/energy

The 1D local density of photonic states:

$$\rho(\omega_0, x) \propto \sum_n \int_{\omega(k)=\omega_0} \frac{\left|\varepsilon_{n,k}(x)\right|^2}{v_g(k)} dk$$

$$v_g = \frac{d\omega}{dk} \qquad \text{So, if:} \quad \frac{d\omega}{dk} \approx 0 \Longrightarrow v_g \to 0 \Longrightarrow \frac{1}{v_g} \to \infty$$

$$F_P = \frac{\Gamma(\omega, r)}{\Gamma_0(\omega)} = \frac{\rho(\omega_0, r)}{\rho_0}$$

For the conventional cavity:

$$F_P = \frac{3}{4\pi^2}\left(\frac{\lambda}{n}\right)^3 \frac{Q}{V_{mode}}$$

QD-based single photon source: processing and testing chain

QD structure for imaging

P. Holewa, et al. ACS Phot. 9, 7, 2273 (**2022**)

Optical imaging, QDs positioning

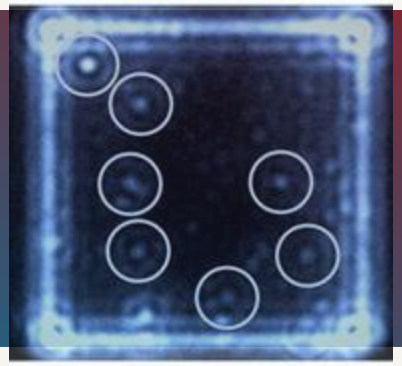

CBG fabrication (EBL+ICP)

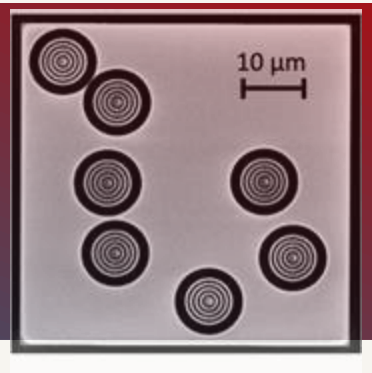

Spectral response

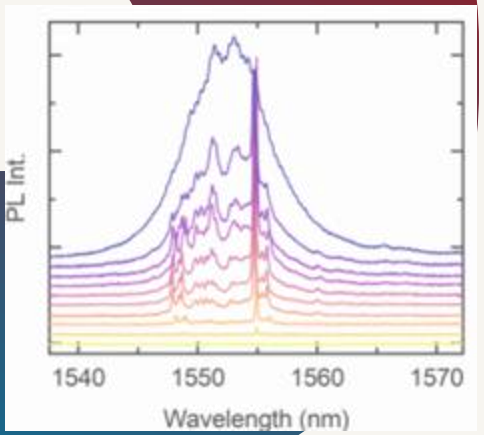

Dynamics/Purcell factor

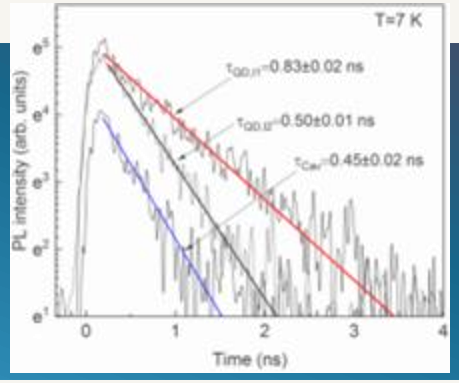

$g^{(2)}(\Delta t)$ – Hunbarry-Brown and Twiss experiment

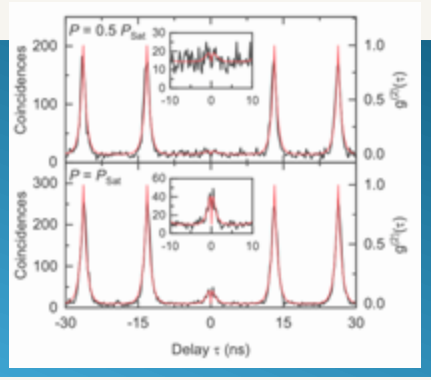

Two photons interference - Hong-Ou-Mandel experiment

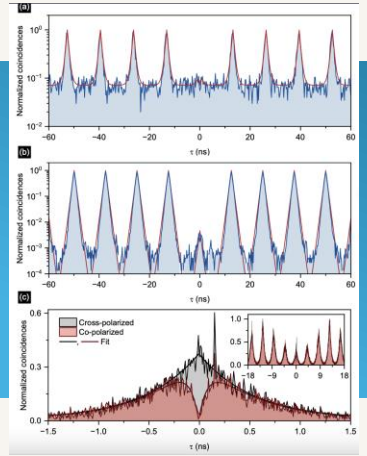

P. Holewa et al. Nature Communications 15, 3358 (**2024**)

Circular Bragg Grating source performance

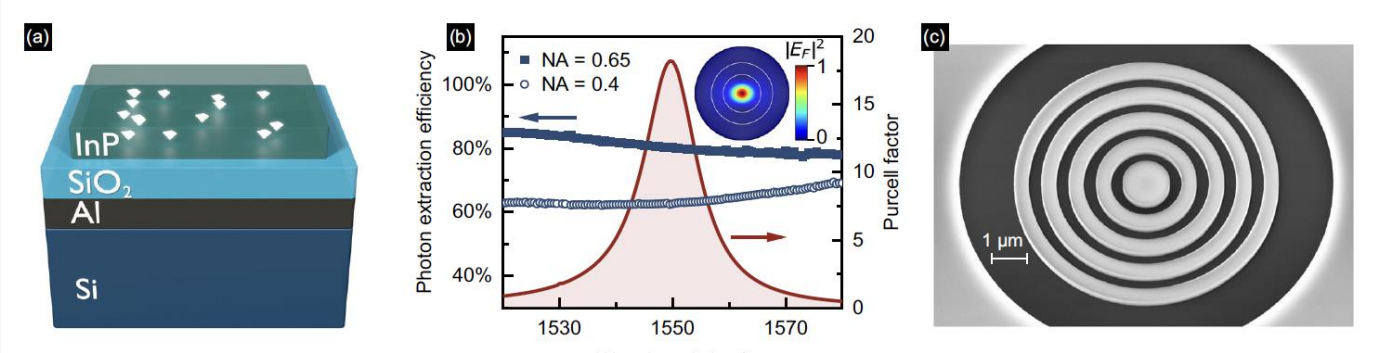

Key parameter	CBG cavity coupled InAs/InP QD
Determistic fabrication/processing yield	YES/24%
Photon extraction efficiency (η)	(16.6 ± 2.7)% (NA=0.64)
Purcell factor (Fp)	(5 ±0.4) (2.0 ns/0.4 ns) (TRPL exp., p-shell exc.)
Single photon purity ($g^{(2)}(0)$)	$g^{(2)}(0)=(3.2 \pm 0.6) \times 10^{-3}$ (HBT exp. p-shell exc.)
Photons indistinguishability (V)	(19.3 ± 2.6) % (HOM exp.) - ps. (~99.8) %

QD spatial position with respect to the cavity field distribution is critical

P. Holewa et al. Nature Communications 15, 3358 (**2024**)

Scalibility and integration

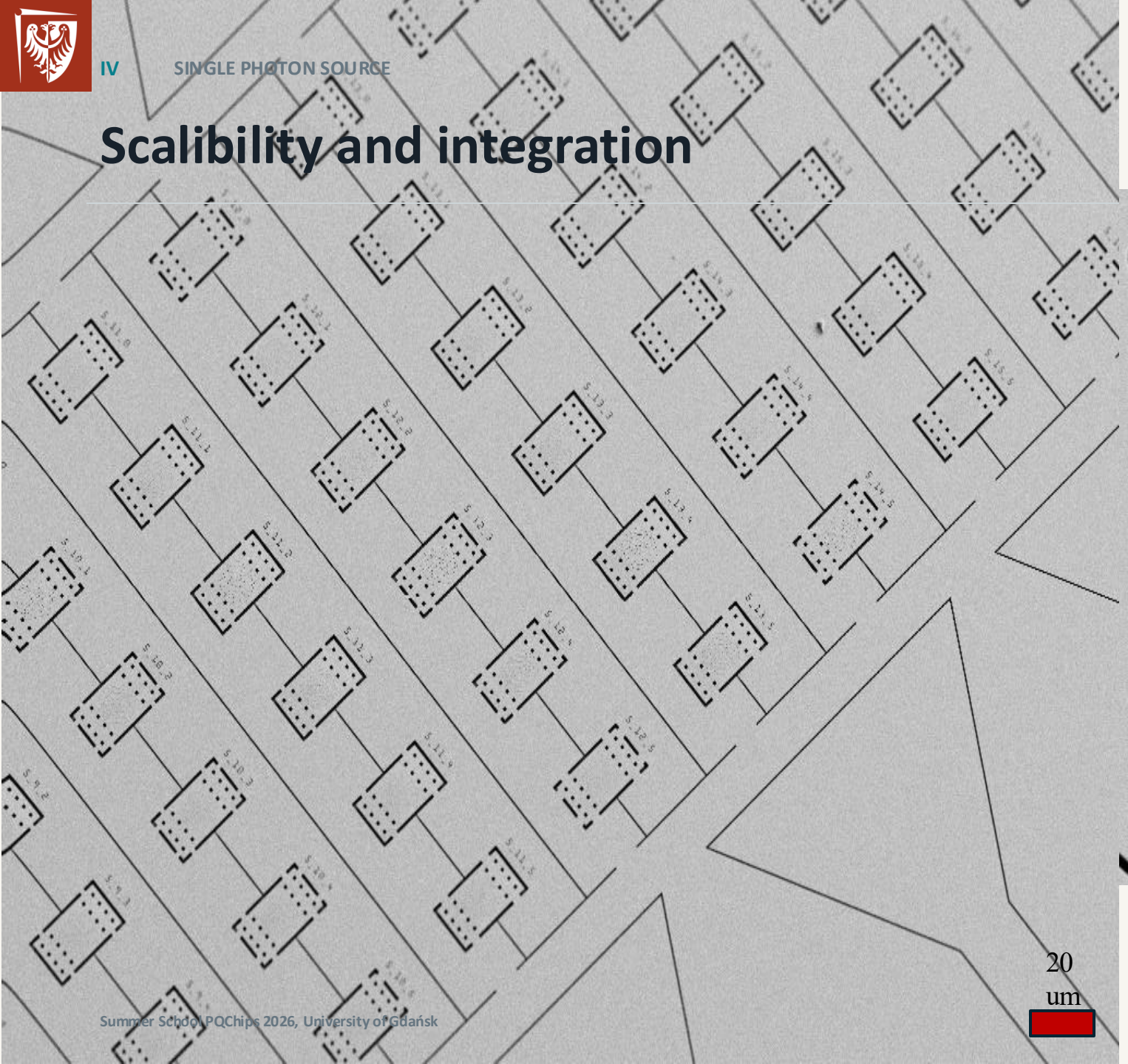

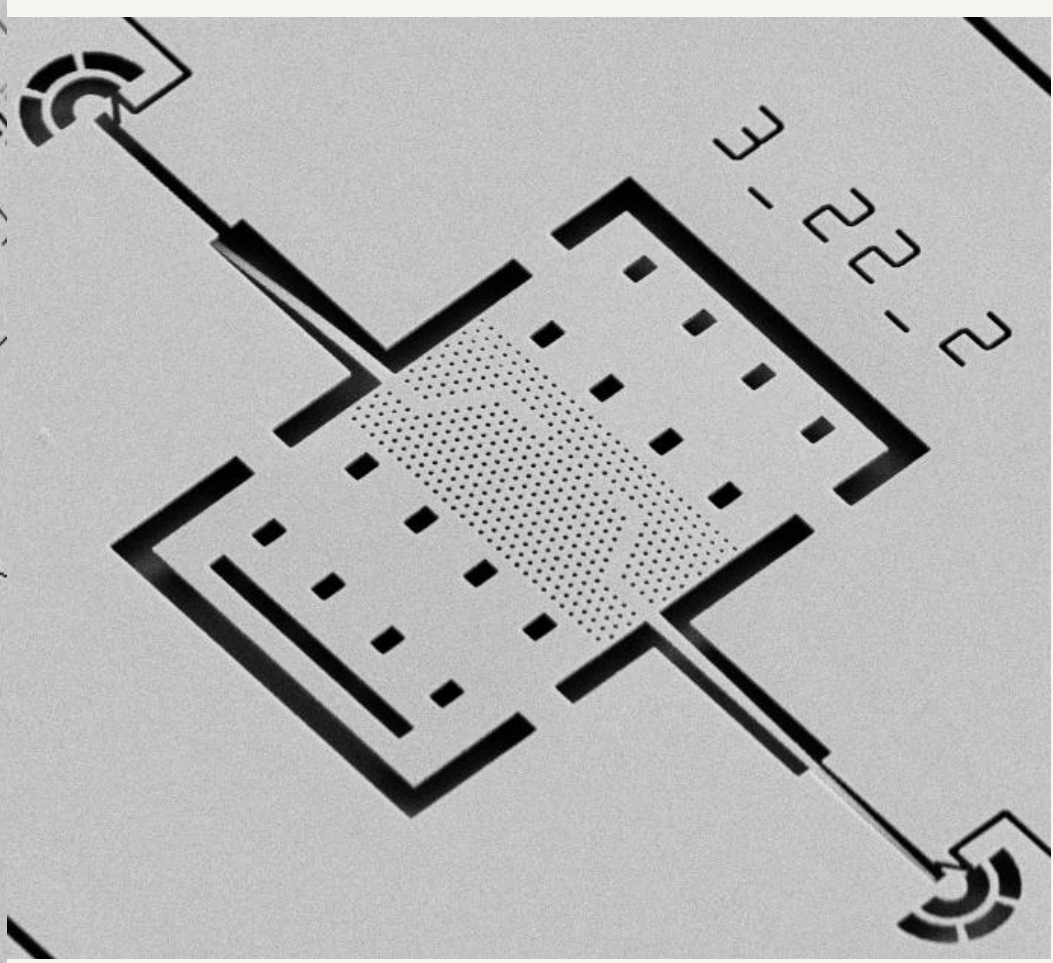

Micro-transfer printing – hybridization of chip components

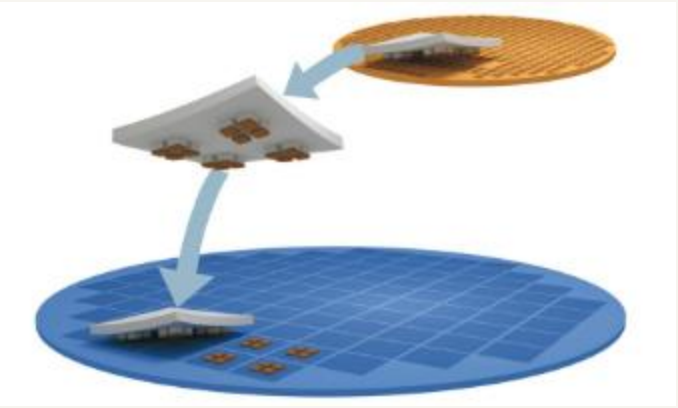

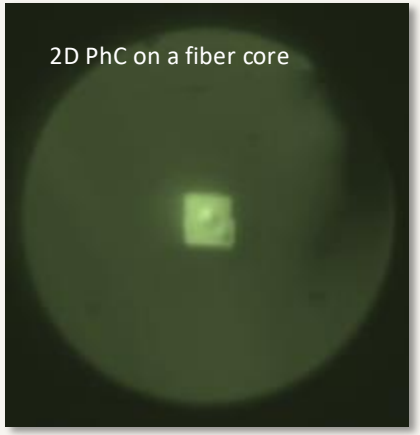

Marek G. Mikulicz et al. Physical Review Applied 24, 014023 (2025)

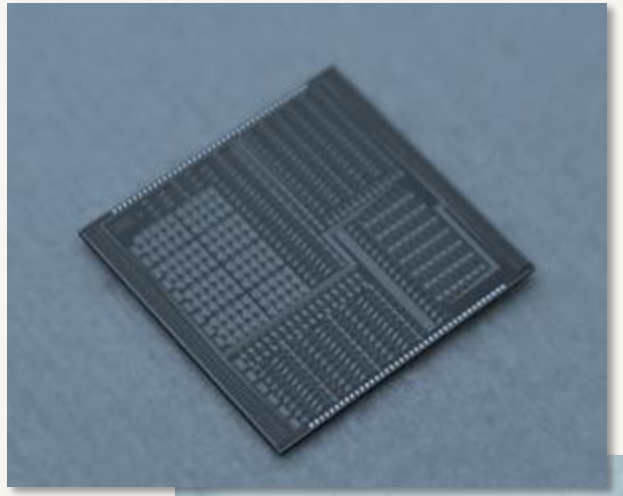

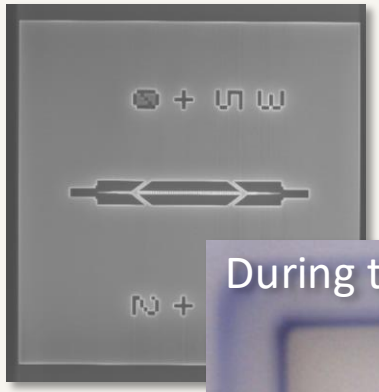

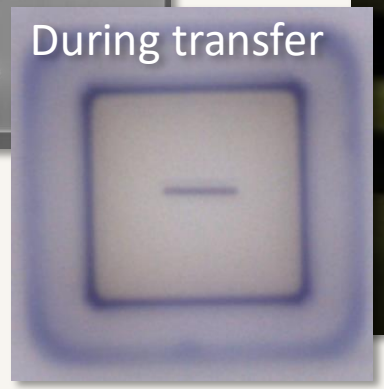

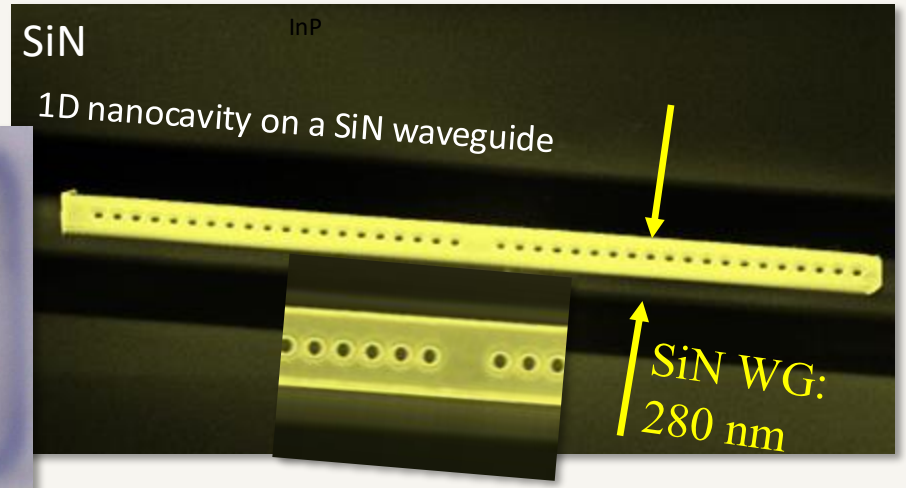

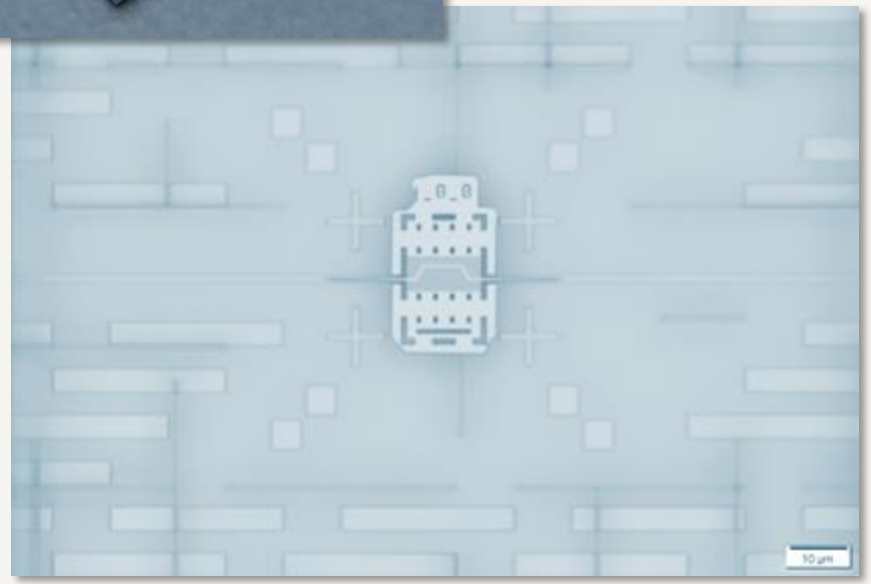

Acknowledgements

Nonlinear Quantum Photonics group

Wrocław University of Science and Technology

Paweł Holewa

Paweł Mrowiński

Mikołaj Badura

Emilia Zięba-Ostój

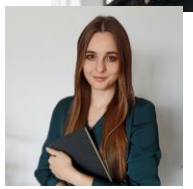

Mikołaj Śmigiel

Marek Mikulicz

Currently PostDoc at: DTU

Dąbrówka Biegańska

Currently PhD at: MONASH University

Patrycja Dembek, Natalia Sanecka, Kacper Pniewski

DTU Electro, Nanodevices Fabrication and Nanoph center

DTU

Nano Photon

Elizaveta Semenova

Kresten Yvind

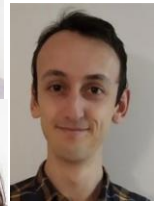

Baptist Lefauher

Karolina Połczyńska

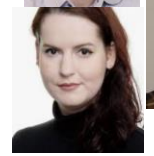

Christian Ruiz

Wrocław University of Science and Technology

Grzegorz Sęk

Tobias Haindle group

Universität Münster

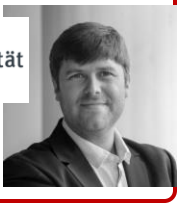

Feng Liu group,
Zhejiang Uni.

QPIC 1550

European Commission

QPIC1550 – Quantum photonic integrated circuits at 1550 nm. **HORIZON-RIA**

NATIONAL SCIENCE CENTRE POLAND

TSUNAMI – deTerministically fabricated, Scalable, bright, and Purcell-enhanced InAs/InP quaNtum dots-based nonclAssical photon sources for quantum communication in the C-band OPUS 2025/57/B/ST7/04916

Integrated quantum photonics on a hybrid InP/SiO2 platform. **SONATA BIS 2023/50/E/ST7/00581**, 2024-2026

Heterogeneous waveguide structures on the Si platform with InAs/InP quantum dots emitting in the 1.55 um spectr range for application in scalable photonic circuits. **SONATA 2020/39/D/ST5/02952**, 2021-2024

NAWA POLISH NATIONAL AGENCY FOR ACADEMIC EXCHANGE

COSMOS – Coherent Single-Photon Sources Integrated with Low-Loss Platforms for Quantum Computing at Telecom Wavelengths.